Collaborative Research Center TRR 257

Particle Physics Phenomenology after the Higgs Discovery

Finite-Quark-Mass Effects on the Higgs Production Cross Section in the Gluon-Gluon Fusion Channel

Dissertation

zur Erlangung des Doktorgrades an der Fakultät für Mathematik, Informatik und Naturwissenschaften

Fachbereich Physik der Rheinisch-Westfälischen Technischen Hochschule

vorgelegt von

Tom Claus Rudolf Schellenberger

Aachen
1. Juli 2025

GUTACHTER DER DISSERTATION:

Prof. Dr. Michał Czakon
Prof. Dr. Robert Harlander

ZUSAMMENSETZUNG DER PRÜFUNGSKOMMISSION:

Prof. Dr. Michał Czakon
Prof. Dr. Robert Harlander
TBA
TBA

VORSITZENDER DER PRÜFUNGSKOMMISSION:

TBA

DATUM DER DISPUTATION:

TBA

DEKAN DER FAKULTÄT MIN:

Prof. Dr. Carsten Honerkamp

ABSTRACT

This is my Abstract

ZUSAMMENFASSUNG

Dies ist meine Zusammenfassung

ACKNOWLEDGMENTS

Here is where I thank god.

PUBLICATIONS

During my PhD studies, I co-authored the following publications:

[1] Michał Czakon, Felix Eschment, and Tom Schellenberger. "Revisiting the double-soft asymptotics of one-loop amplitudes in massless QCD." In: *JHEP* 04 (2023), p. 065. DOI: 10.1007/JHEP04(2023)065. arXiv: 2211.06465 [hep-ph]

[2] Michał Czakon, Felix Eschment, and Tom Schellenberger. "Subleading effects in soft-gluon emission at one-loop in massless QCD." In: *JHEP* 12 (2023), p. 126. DOI: 10.1007/JHEP12(2023)126. arXiv: 2307.02286 [hep-ph]

[3] Michał Czakon et al. "Top-Bottom Interference Contribution to Fully Inclusive Higgs Production." In: *Phys. Rev. Lett.* 132.21 (2024), p. 211902. DOI: 10.1103/PhysRevLett.132.211902. arXiv: 2312.09896 [hep-ph]

[4] Michał Czakon et al. "Quark mass effects in Higgs production." In: *JHEP* 10 (2024), p. 210. DOI: 10.1007/JHEP10(2024)210. arXiv: 2407.12413 [hep-ph]

Among these, only the last two are directly relevant to this dissertation.

CONTENTS

ACRONYMS

SM	Standard model
VEV	Vacuum expectation value
SSB	Spontaneous symmetry breaking
PDF	Parton distribution function
QCD	Quantum chromodynamics
QED	Quantum electrodynamics
RGE	Renormalization group equation
LO	Leading order
DR	Dimensional regularization
UV	Ultraviolet
IR	Infrared
LO	Leading order
NLO	Next-to-leading order
NNLO	Next-to-next-to-leading order
OS	On-shell renormalization
RG	Renormalization group
RGE	Renormalization group equation
LHC	Large hadron collider
FS	Flavor scheme
MC	Monte-Carlo
LME	Large mass expansion
HEL	High-energy limit
HTL	Heavy-top limit
rHTL	Rescaled heavy-top limit
SCET	Soft-collinear effective theory

NOTATION, CONSTANTS AND CONVENTIONS

- In this thesis, I will be using the *Einstein summation convention*, by which any index—be it a Lorentz, color or flavor index—which appears twice is implicitly summed over.
- I will be using natural units
$$\hbar = c = 1. \tag{0.1}$$
- The electron charge is
$$-e, \quad e > 0. \tag{0.2}$$
- The metric is
$$g_{\mu\nu} = \begin{pmatrix} 1 & & & \\ & -1 & & \\ & & -1 & \\ & & & -1 \end{pmatrix}. \tag{0.3}$$
- The normalization of the Levi-Civita anti-symmetric tensor $\epsilon_{\mu\nu\rho\sigma}$ is
$$\epsilon_{0123} = +1 \tag{0.4}$$
- The Pauli matrices are defined as
$$\sigma^1 \equiv \begin{pmatrix} 0 & 1 \\ 1 & 0 \end{pmatrix}, \quad \sigma^2 = \begin{pmatrix} 0 & -i \\ i & 0 \end{pmatrix}, \quad \sigma^3 = \begin{pmatrix} 1 & 0 \\ 0 & -1 \end{pmatrix}, \quad \tau^i \equiv \sigma^i. \tag{0.5}$$
- Unless specifically specified otherwhise we will use the following values for appearing physical constants
  - $G_F = 1.16637 \times 10^{-5}$ GeV^{-2}
  - $m_H = 125.00$ GeV
  - $m_t = 173.06$ GeV
  - $\overline{m}_t(\overline{m}_t) = 162.7$ GeV
  - $m_b = 4.18$ GeV
  - $\overline{m}_b(\overline{m}_b) = 2.41$ GeV
  - $m_c = 1.27$ GeV
  - $m_Z = 91.1876$ GeV
- We use the `NNPDF31_nnlo_as_0118` and `NNPDF31_nnlo_as_0118_nf_4`PDF set in the 5FS and 4FS respectively.
- α_s is extracted from the PDF set at the Z^0 mass.

1 | INTRODUCTION

General introductions

2 THE STANDARD MODEL OF PARTICLE PHYSICS

2.1 ELECTROWEAK SYMMETRY BREAKING

The standard model (SM) of particle physics is a theory describing all known matter and their fundamental interactions except for gravity. It unifies the electromagnetic, weak, and strong forces under a single theoretical framework. The matter content of the SM is classified into two primary groups: *fermions* and *bosons*. The fermions have spin 1/2, they are further subcategorized into *quarks* and *leptons*. Quarks participate in strong interactions, while leptons interact only via the electromagnetic and weak forces. In contrast, bosons have integer spin. There exists a single particle with spin 0, the *Higgs* boson, and four vector bosons, namely the gluon, the photon, and the W and Z boson. The vector bosons act as force carrier for the strong, the electromagnetic and the weak force respectively. Fermions are organized into three generations, with each generation containing two types of quarks (up-type and down-type) and two leptons (a charged lepton and its corresponding neutrino). These generations are shown in Fig. 2.1, along with their masses, charges, and spins.

The interactions between SM particles are described by a non-abelian gauge theory of the $\mathrm{SU}(3)_C \times \mathrm{SU}(2)_L \times \mathrm{U}(1)_Y$ group. Here $\mathrm{SU}(3)_C$ governs the strong interactions. It applies to all *colored* particles, i.e. quarks and gluons. The quarks transform under the fundamental representation of the $\mathrm{SU}(3)_C$ group. $\mathrm{SU}(2)_L \times \mathrm{U}(1)_Y$ governs electroweak interactions. The $\mathrm{SU}(2)_L$ transformation acts non-trivially only on *left-handed* fermions which form doublets

$$\begin{gathered} L_{iL} \equiv \begin{pmatrix} \nu_{iL} \\ l_{iL} \end{pmatrix}, \quad Q_{iL} \equiv \begin{pmatrix} u_{iL} \\ d_{iL} \end{pmatrix}, \\ \nu_i = (\nu_e, \nu_\mu, \nu_\tau)\,, \quad l_i = (e, \mu, \tau)\,, \quad u_i = (u, c, t)\,, \quad d_i = (d, s, b)\,. \end{gathered} \tag{2.1}$$

The phase transformation $\mathrm{U}(1)_Y$ acts on all particles except neutrinos according to their quantum number, the *hypercharge* Y. The symmetry is spontaneously broken to $\mathrm{SU}(3)_C \times \mathrm{U}(1)_Q$, where the $\mathrm{U}(1)_Q$ group corresponds to gauge transformation of the electromagnetic interaction, hence the subscript Q for the *electric charge*. To ensure that the particles have the correct charges, the hypercharge must satisfy the *Gell-Mann–Nishijima relation*:

$$\frac{Y}{2} = Q - I^3. \tag{2.2}$$

With the particle charges displayed in Fig. 2.1 we then get

	L_{iL}	Q_{iL}	ν_{iR}	l_{iR}	u_{iR}	d_{iR}
$\frac{Y}{2}$	$-\frac{1}{2}$	$\frac{1}{6}$	0	-1	$\frac{2}{3}$	$-\frac{1}{3}$

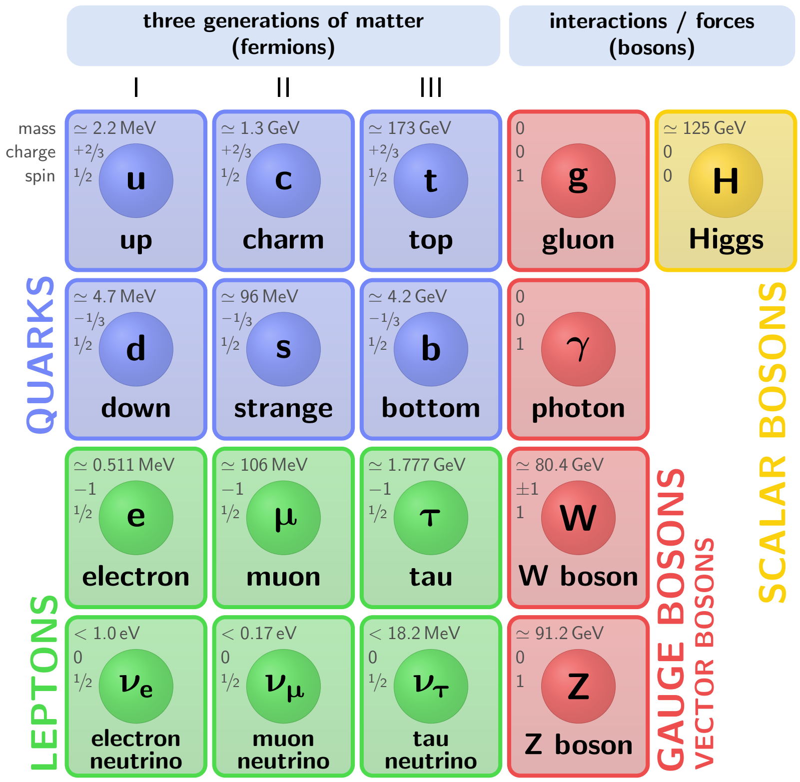

Figure 2.1: Elementary particles of the SM. The was image generated with the help of Ref. [5].

The transformation properties of the gauge bosons is dictated by the covariance of the covariant derivative

$$
\begin{gathered}
D_\mu \equiv \partial_\mu - igA^a_\mu T^a_R - ig_2 W^a_\mu I^a + ig_Y \frac{Y}{2} B_\mu \\
T^a_R = \begin{cases} T^a & \text{for quarks,} \\ 0 & \text{for leptons,} \end{cases} \qquad I^a = \begin{cases} \frac{\tau}{2} & \text{for left-handed fermions,} \\ 0 & \text{for right-handed fermions,} \end{cases}
\end{gathered} \tag{2.3}
$$

where T^a and τ^a are the *Gell-Mann* and *Pauli* matrices.

Before spontaneous symmetry breaking, the Lagrangian which governs the evolution of all matter fields must be invariant under the $\mathrm{SU}(3)_C \times \mathrm{SU}(2)_L \times \mathrm{U}(1)_Y$ gauge group. Up to a $\mathbb{CP}$ violating term[1] the SM Lagrangian is the most general mass-dimension four Lagrangian for the described particle content

$$
\mathcal{L}_{\mathrm{SM}} = \mathcal{L}_G + \mathcal{L}_F + \mathcal{L}_Y + \mathcal{L}_H . \tag{2.4}
$$

1 The absence of the $\mathbb{CP}$ violating term $\theta \frac{g^2}{64\pi^2} \epsilon^{\mu\nu\alpha\beta} F^a_{\mu\nu} F^a_{\alpha\beta}$ is an unsolved problem of particle physics, known as the strong CP problem.

The gauge-field Lagrangian $\mathcal{L}_G$ describes the free propagation and in the case of the non-abelian groups $\mathrm{SU}(3)_C$ and $\mathrm{SU}(2)_L$ also the self-interaction of the gauge bosons. It is given by

$$
\begin{aligned}
\mathcal{L}_G = -\frac{1}{4}G^a_{\mu\nu}G^{a\,\mu\nu} - \frac{1}{4}W^a_{\mu\nu}W^{a\,\mu\nu} - \frac{1}{4}B_{\mu\nu}B^{\mu\nu}, \\
G^a_{\mu\nu} \equiv \partial_\mu A^a_\nu - \partial_\nu A^a_\mu + g f^{abc} A^b_\mu A^c_\nu, \\
W^a_{\mu\nu} \equiv \partial_\mu W^a_\nu - \partial_\nu W^a_\mu + g_2 \epsilon^{abc} W^b_\mu W^c_\nu, \\
B_{\mu\nu} \equiv \partial_\mu B_\nu - \partial_\nu B_\mu.
\end{aligned}
\tag{2.5}
$$

The propagation of the fermions and their interaction with the gauge bosons is described by

$$
\mathcal{L}_F = \bar{L}_{iL} i \not{D} L_{iL} + \bar{\nu}_{iR} i \not{D} \nu_{iR} + \bar{l}_{iR} i \not{D} l_{iR} + \bar{Q}_{iL} i \not{D} Q_{iL} + \bar{u}_{iR} i \not{D} u_{iR} + \bar{d}_{iR} i \not{D} d_{iR}. \tag{2.6}
$$

The Higgs field is a doublet of the $\mathrm{SU}(2)_L$ group. We want the field to have a non-vanishing vacuum expectation value (VEV) to dynamically generate the fermion and boson masses. Of course, the vacuum cannot carry an electric charge, which means that the Higgs field must be electrically neutral along the direction of *spontaneous symmetry breaking* (SSB). We choose this to be the second component of the doublet. With the Gell-Mann–Nishijima relation we can then deduce that hypercharge of the doublet must be $Y = +1$. The Higgs doublet field thus takes the form

$$
\Phi = \begin{pmatrix} \phi^+ \\ \phi^0 \end{pmatrix}, \tag{2.7}
$$

where the superscript indicates the electic charge.

In order to generate a non-vanishing VEV, the Higgs field must be in a potential with a global minimum away from zero. Hence, the only gauge invariant mass-dimension four Lagrangian we can construct is

$$
\begin{aligned}
\mathcal{L}_H = (D_\mu \Phi)^\dagger (D^\mu \Phi) - V(\Phi) \\
V(\Phi) = \lambda(\Phi^\dagger\Phi)^2 - \mu^2 \Phi^\dagger \Phi, \quad \mu^2, \lambda > 0.
\end{aligned}
\tag{2.8}
$$

The minimum of the Higgs potential V is at

$$
\Phi_0^\dagger \Phi_0 = \frac{\mu^2}{2\lambda} \equiv \frac{v^2}{2} \neq 0. \tag{2.9}
$$

After (SSB) we can expand the Higgs field around its minimum

$$
\Phi = \begin{pmatrix} \phi^+ \\ \frac{1}{\sqrt{2}}(v + H + i\xi). \end{pmatrix} \tag{2.10}
$$

The real scalar field H is the famous Higgs boson, whereas the fields $\phi^\pm$ and ξ are unphysical since they can always be eliminated through a gauge transformation (*would-be Goldstone bosons*). After inserting the expansion in the Higgs Lagrangian, the mass of the Higgs can be read off from its square term

$$
m_H = \sqrt{2}\mu. \tag{2.11}
$$

SSB enables the generation of vector boson masses without breaking the gauge symmetry explicitly. If we insert the expanded Higgs field in the Higgs Lagrangian, we get quadratic terms of the gauge boson fields

$$\begin{aligned}\mathcal{L}_H \supsetneq \frac{v^2}{2}&\left\{g_2^2 \begin{pmatrix}0 & 1\end{pmatrix} I^a I^b \begin{pmatrix}0\\1\end{pmatrix} W^a_\mu W^{b\,\mu} - g_2 g_Y \begin{pmatrix}0 & 1\end{pmatrix} I^a \begin{pmatrix}0\\1\end{pmatrix} W^a_\mu B^\mu + \frac{g_Y^2}{4} B_\mu B^\mu\right\}\\ = \frac{v^2}{2}&\left\{\frac{g_2^2}{4}\left[(W^1)^2 + (W^2)^2\right] + \frac{1}{4}\begin{pmatrix}B^\mu & W^{3\,\mu}\end{pmatrix}\begin{pmatrix}g_Y^2 & g_Y g_2\\ g_Y g_2 & g_2^2\end{pmatrix}\begin{pmatrix}B_\mu\\ W^3_\mu\end{pmatrix}\right\}.\end{aligned} \tag{2.12}$$

By diagonalizing the mass matrix we obtain the physical states

$$\begin{pmatrix}A^\gamma_\mu\\ Z_\mu\end{pmatrix} = \begin{pmatrix}\cos\theta_W & -\sin\theta_W\\ \sin\theta_W & \cos\theta_W\end{pmatrix}\begin{pmatrix}B_\mu\\ W^3_\mu\end{pmatrix}, \quad \cos\theta_W = \frac{g_2}{\sqrt{g_Y^2+g_2^2}}, \sin\theta_W = \frac{g_Y}{\sqrt{g_Y^2+g_2^2}}. \tag{2.13}$$

In this new basis, we have one massless boson A^γ_μ, which we identify as the photon and a charge neutral boson of mass

$$m_Z = \frac{v}{2}\sqrt{g_Y^2+g_2^2}. \tag{2.14}$$

The vector bosons W^1 and W^2 are not eigenstates of the charge operator. We therefore define the new states

$$W^\pm_\mu = \frac{1}{\sqrt{2}}\left(W^1_\mu \mp i W^2_\mu\right), \qquad Q W^\pm_\mu = \pm W^\pm_\mu, \tag{2.15}$$

which are eigenstates of Q and have mass

$$m_W = \frac{v}{2} g_2. \tag{2.16}$$

Last but not least, we discuss the Yukawa sector of the SM Lagrangian. Before SSB, fermions cannot generate masses because a mass term would mix the left- and right-handed components of the fields, thereby breaking the chiral gauge symmetry. Here, once again, the Higgs field comes to the rescue: by coupling the fermions with the Higgs field through a Yukawa interaction[2]

$$\mathcal{L}_Y = -\left(y^\nu_{ij}\bar{L}_{iL}\Phi^c\nu_{jR} + y^l_{ij}\bar{L}_{iL}\Phi l_{jR} + y^d_{ij}\bar{Q}_{iL}\Phi d_{jR} + y^u_{ij}\bar{Q}_{iL}\Phi^c u_{jR}\right) + \text{h.c.}, \tag{2.17}$$

where Φ^c is the charge-conjugated field to Φ, we do not explicitly break the symmetry. However, after SSB this Lagrangian will generate exactly the required mixing between left- and right-handed fields to generate the fermion masses. The Yukawa-interaction matrices $y^{\nu,l,d,u}_{ij}$ can be shifted from the Yukawa sector to the fermion sector through a field redefinition. Indeed, if we apply the *singular value decomposition* of the Yukawa matrix

$$y = U_L^\dagger y_{\text{diag}} U_R, \quad \text{with} \quad (y_{\text{diag}})_{ij} = \sqrt{2} Y_i \delta_{ij} \quad \text{and} \quad U_{L,R} \in \mathrm{U}(3), \tag{2.18}$$

and redefine our fermion fields to be

$$f_{iR} \longrightarrow U_{Rij} f_{jR}, \qquad f_{iL} \longrightarrow U_{Lij} f_{jL}, \qquad f = \nu, l, u, d \tag{2.19}$$

the Yukawa Lagrangian becomes

$$\mathcal{L}_Y = -\sum_i \left(m_{\nu_i}\bar{\nu}_i\nu_i + m_{l_i}\bar{l}_i l_i + m_{u_i}\bar{u}_i u_i + m_{d_i}\bar{d}_i d_i\right)\left(1 + \frac{H}{v}\right). \tag{2.20}$$

2 In the original formulation of the SM, there are no neutrino Yukawa interactions, since they were believed to be massless. Neutrino oscillation experiments have shown however, that neutrinos do in fact have finite masses.

Here we identified the Yukawa coupling as $Y_i = m_i/v$ in order to generate the required mass terms. Consequently, we observe that the Yukawa coupling of the Higgs to the fermions is proportional to the mass of that fermion. The field redefinition is a change from a flavor eigenbasis, which is diagonal in the couplings to the gauge bosons, to a mass eigenbasis. In the mass eigenbasis the part of fermion Lagrangian which contains the interaction to the electroweak gauge bosons after SSB is

$$\begin{aligned}\mathcal{L}_F \supsetneq & \sum_f (-Q_f) e \bar{f}_i \not{A}^\gamma f_i + \sum_f \frac{e}{\sin\theta_W \cos\theta_W} \bar{f}_i (I_f^3 \gamma^\mu P_L - \sin^2\theta_W Q_f \gamma^\mu) f_i Z_\mu \\ & + \frac{e}{\sqrt{2}\sin\theta_W} \left(\bar{u}_i \gamma^\mu P_L (V_{\mathrm{CKM}})_{ij} d_j W_\mu^+ + \bar{d}_i \gamma^\mu P_L (V_{\mathrm{CKM}}^\dagger)_{ij} u_j W_\mu^- \right) \\ & + \frac{e}{\sqrt{2}\sin\theta_W} \left(\bar{\nu}_i \gamma^\mu P_L (V_{\mathrm{PMNS}}^\dagger)_{ij} l_j W_\mu^+ + \bar{l}_i \gamma^\mu P_L (V_{\mathrm{PMNS}})_{ij} \upsilon_j W_\mu^- \right).\end{aligned} \tag{2.21}$$

Here we identified the electromagnetic coupling constant

$$e = \frac{g_2 g_Y}{\sqrt{g_2^2 + g_Y^2}}, \tag{2.22}$$

as the factor in front of the photon interaction term. The operators $P_{L,R}$ are just the projectors onto the left- and right-handed components

$$P_{L,R} = \frac{1 \mp \gamma^5}{2}. \tag{2.23}$$

The *CKM* and *PMNS matrices*[3] are the results of the field redefinitions

$$V_{\mathrm{CKM}} \equiv U_L^{u\dagger} U_L^d, \qquad V_{\mathrm{PMNS}} \equiv U_L^{l\,\dagger} U_L^\nu. \tag{2.24}$$

Typically, one prefers to work in the mass eigenbasis of the quarks, while the neutrinos are kept in the flavor eigenbasis, in which case one encounters flavor changes (*neutrino oscillations*) through propagation. This is why the PMNS matrix is defined in terms of the complex conjugate of the CKM matrix equivalent in the lepton sector.

2.2 CROSS SECTIONS

Cross sections offer the possibility to directly test the SM and many of the great successes of the SM are its *cross section* predictions. The cross section is simply defined as the probability to create some final state from some initial state per unit of time per target particle normalized by the incoming particle flux. This definition allows for straightforward measurement through counting experiments. For instance, experiments like `CMS` and `ATLAS` collide particles and count how often a particular final state is produced within a given time interval.

From a theoretical perspective, cross sections can be calculated using

$$\mathrm{d}\hat{\sigma}_{ij\to n} = \frac{1}{F} \mathrm{d}\Phi_n |M_{ij\to n}|^2, \tag{2.25}$$

where F denotes the *flux factor*[4]

$$F \equiv 4 p_1 \cdot p_2, \tag{2.26}$$

3 Named after Cabibbo, Kobayashi and Maskawa, and Pontecorvo, Maki, Nakagawa and Sakata.
4 In the following we assume that the initial state particles are massless.

$\mathrm{d}\Phi_n$ is the *Lorentz invariant phase space measure*

$$\mathrm{d}\Phi_n = \left[\prod_{i=1}^{n} \frac{\mathrm{d}^4 q_i}{(2\pi)^4}(2\pi)\delta(q_i^2 - m_i^2)\Theta(q_i^0)\right](2\pi)^4\delta^{(4)}\left(p_1 + p_2 - \sum_{i=1}^{n} q_i\right), \tag{2.27}$$

and M_{fi} is the *scattering amplitude* describing the short distance interactions.

The computation of cross sections involves three basic steps:

1. Calculation of the hard scattering amplitude,
2. Phase-space integration,
3. And the convolution with *parton distribution functions* (PDFs).

We will discuss each step in detail below.

2.2.1 The Hard Scattering Amplitude

The Hard Scattering Amplitude describes the transition probability from a specific initial state to a particular finial state. Since the scattering is **hard**, it implies that the energy transfer between particles during scattering is large compared to the QCD scale. Thus, we operate within the perturbative regime of QCD and can perform an expansion in terms of the coupling constant

$$M_{ij\to n} = \alpha_s^{n_{\mathrm{Born}}}\left(M_{ij\to n}^{(0)} + \frac{\alpha_s}{\pi}M_{ij\to n}^{(1)} + \left(\frac{\alpha_s}{\pi}\right)^2 M_{ij\to n}^{(2)} + \mathcal{O}\left(\alpha_s^3\right)\right). \tag{2.28}$$

Here, n_{Born} denotes the power of the coupling constant at *leading order* (LO). The coefficients in this series can be computed graphically using *Feynman rules*. These are the set of all allowed propagators and vertices together with the corresponding mathematical prescription. The Feynman rules for the complete SM are listed in Appendix A. To calculate the coefficient $M_{ij\to n}^{(l)}$ for a specific process, one has to draw all possible connected and amputated Feynman diagrams with the initial state (i, j) and final state n, that contain $2(n_{\mathrm{Born}} + l)$ vertices[5]. Then one uses the Feynman rules to get the mathematical translation, keeping in mind that momentum must be conserved at every vertex and also taking into account possible symmetry factors.

Starting from $M_{ij\to n}^{(1)}$, but for some processes, called *loop induced processes*, even from $M_{ij\to n}^{(0)}$, we will encounter loops in the diagrams. Inside a loop, the momentum of the edges cannot be uniquely determined through momentum conservation. Consequently, we must leave momentum unspecified and integrate over all possible values. Typically, it is the computation of these *loop integrals* that makes the calculation of hard scattering amplitudes so challenging. A plethora of powerful techniques has been developed over the years to tackle this daunting task. Still, the computation of loop integrals remains a highly active field of research and two-loop amplitudes with 5 or more scales are only just becoming available. A detailed description of modern techniques is beyond the scope of this thesis. For a comprehensive overview see Ref. [6].

Loop integrals are notorious for exhibiting divergences. To tame these, we introduce *regulators*, i.e. we introduce a parameter, such that the integral becomes function of that parameter with a singularity at the physical value. The most commonly used regularization scheme is

5 Quartic vertices are counted twice.

dimensional regularization (DR), here we make the loop-integral a function of the dimension by replacing

$$\int \frac{\mathrm{d}^4 k}{(2\pi)^4} (\cdots) \longrightarrow \bar{\mu}^{2\epsilon} \int \frac{\mathrm{d}^d k}{(2\pi)^d} (\cdots), \quad d \equiv 4 - 2\epsilon \in \mathbb{C}, \quad \gamma_E = 0.5772\ldots. \tag{2.29}$$

The dimensionally regularized integral satisfies the usual integral properties like linearity, translation invariance and rescaling. The mass scale,

$$\bar{\mu}^2 = \frac{\mu^2}{4\pi} e^{\gamma_E} \tag{2.30}$$

was introduced to retain the mass dimension of the measure to 4, while absorbing some common factors of loop integrals. The physical limit then corresponds to $\epsilon \to 0$. A divergent integral in four dimensions will hence have ϵ-poles in DR. The poles are categorized as *ultraviolet* poles if their origin are large loop momenta, i.e. the four dimensional integral diverges for $k \to \infty$. Further we categorize poles as *infrared* poles if the singularity arises from loop momenta which are either soft ($k \to 0$) or *collinear* ($k \cdot p_i \to 0$) to one of the external massless legs. UV and IR singularities are mutually exclusive since they originate from different regions of the phase space. This means that the poles do not multiply together, and we may only get a single UV pole per loop integration. The soft and collinear singularities are **not** exclusive, meaning that IR singularities can develop one double pole per loop integration.

The IR singularities cancel for inclusive observables as we shall discuss in detail in section 2.2.3. UV poles on the other hand, are removed through a method called *renormalization*. Renormalization hinges on the idea, that the fields, constants and masses we observe in nature are not necessarily the same as the one in our Lagrangian. Instead, they are related through a *renormalization constant*

$$\begin{aligned}
W_\mu^{B,a} &= \left(Z_3^W\right)^{1/2} W_\mu^{R,a} \\
B_\mu^B &= \left(Z_3^Z\right)^{1/2} B_\mu^R \\
A_\mu^{B,a} &= \left(Z_3^A\right)^{1/2} A_\mu^{R,a} \\
\Phi^B &= \left(Z^\Phi\right)^{1/2} \Phi^R \\
Q_{iL}^B &= \left(Z_{2i}^L\right)^{1/2} Q_{iL}^R \\
u_{iR}^{B,a} &= \left(Z_{2i}^{u,R}\right)^{1/2} u_{iR}^{B,a} \\
d_{iR}^{B,a} &= \left(Z_{2i}^{d,R}\right)^{1/2} d_{iR}^{B,a} \\
g^B &= Z_g g^R \\
g_Y^B &= Z_Y g_Y^R \\
g_2^B &= Z_2 g_2^R \\
\left(\mu^2\right)^B &= Z_\mu \left(\mu^2\right)^R \\
\lambda^B &= Z_\lambda \lambda^R \\
y_{ij}^{d,B} &= Z_{y,ij}^d y_{ij}^{d,R} \\
y_{ij}^{u,B} &= Z_{y,ij}^u y_{ij}^{u,R}
\end{aligned} \tag{2.31}$$

In these equations B refers to *bare* quantities appearing within our Lagrangian while R signifies renormalized quantities that are finite by definition. In the SM, it can be shown [7, 8] that we can choose renormalization constants, such that *Green's functions*, i.e. vacuum expectation values of time ordered products of local renormalized fields, are free of UV divergences. Scattering amplitudes, generally do not depend on the unphysical fields, which is why the fields can be kept unrenormalized in this case. Since at LO Green's functions do not require renormalization, all renormalization constants are equal to the identity at this order.

The definition of the renormalization constants is not unique. Indeed, the renormalization constants were designed to absorb singularities, but the finite part is a priori unconstrained. We call a prescription which uniquely determines the renormalization constants a *renormalization scheme*. The most widely used renormalization scheme is the $\overline{\mathrm{MS}}$ scheme. Here, beyond the leading 1 and a universal factor of $\bar{\mu}^{\epsilon\rho_i}$, the renormalization constants **only** consist of poles, i.e. the renormalization constants have the structure

$$Z_i(\alpha) = \bar{\mu}^{\epsilon\rho_i}\left(1 + \frac{z_1}{\epsilon}\frac{\alpha}{4\pi} + \left(\frac{z_{22}}{\epsilon^2} + \frac{z_{21}}{\epsilon}\right)\left(\frac{\alpha}{4\pi}\right)^2 + \dots\right). \tag{2.32}$$

ρ_i is the mass dimension of the operator in units of ϵ, so that the factor $\bar{\mu}^{\epsilon\rho_i}$ corrects for the mismatch in mass dimensions between the four-dimensional renormalized and the d-dimensional bare quantities. For example: the coupling constant g^B has mass dimension ϵ, hence the renormalized coupling g^R has mass dimension zero and $\rho_i = 1$.

$\overline{\mathrm{MS}}$-renormalized masses are generally different from the pole mass. The *on-shell renormalization* (OS) scheme, is an alternative to the $\overline{\mathrm{MS}}$ scheme specifically designed, such that the renormalized mass matches the pole mass. It is therefore the suitable choice for external particles that are asymptotically free. Bare quantities are independent of the chosen renormalization scheme. The invariance under the change of the renormalization scheme defines a group, the *renormalization group* (RG). In the $\overline{\mathrm{MS}}$ scheme, the change from one scale $\bar{\mu}$ to another defines a continuous subgroup of the RG. This means we can formulate the invariance in terms of a differential equation

$$0 = \frac{\mathrm{d}}{\mathrm{d}\log\mu}a^B = a^R\frac{\mathrm{d}Z_a^{\overline{\mathrm{MS}}}}{\mathrm{d}\log\mu} + Z_a^{\overline{\mathrm{MS}}}\frac{\mathrm{d}a^R}{\mathrm{d}\log\mu}, \tag{2.33}$$

where a could be a mass or a coupling. Eq. (2.33) is called the *renormalization group equation* (RGE) and it can be leveraged to determine the scale dependence, also called the *running*, of the observable.

The final step in calculating the hard scattering amplitude involves the application of the *Lehmann-Symanzik-Zimmermann* (LSZ) reduction formula. It relates the scattering amplitudes to Green's functions, and it is the reason why we only considered amputated Feynman diagrams. In practice, one just has to multiply each external field with the square root of the corresponding LSZ constant. These constants are defined as the proportionality factor between the propagator of the interacting and the free theory[6]. As such, they are numerically identical to the OS field renormalization constants.

6 The interacting field theory might have an additional continuous spectrum.

2.2.2 The Parton Distribution Functions

In hadron collisions, the initial state is not made up of elementary particles, but are bound states thereof. This means that during an inelastic scattering event, the partons which take part in the short-range interaction only carry a fraction of the original hadron momentum

$$p_1 = x_1 P_1, \qquad p_2 = x_2 P_2. \tag{2.34}$$

Here p_1 and p_2 denote the momenta of the partons and P_1 and P_2 are the momenta of the hadrons. Since the momentum of the parton can not be larger than that of the hadron, $x_{1,2}$ is restricted to be less than one. Furthermore, since the energy of the parton must be positive the momentum fraction must also be positive. Otherwise, the momentum fraction is a priori unconstrained, we therefore integrate over all allowed values of x_1 and x_2

$$\begin{aligned} \mathrm{d}\sigma_{H_1 H_2 \to n}(S) &= \int_0^1 \mathrm{d}x_1 \mathrm{d}x_2\, f_{H_1,i}(x_1) f_{H_2,j}(x_2) \mathrm{d}\hat{\sigma}_{ij\to n}(x_1 P_1, x_2 P_2, \mu_R) \\ &= \int_0^1 \frac{\mathrm{d}\tau}{\tau} \mathcal{L}_{ij}(\tau) \mathrm{d}\hat{\sigma}_{ij\to n}(\tau S, \mu_R) \end{aligned} \tag{2.35}$$

where $S = 2P_1 \cdot P_2$ is hadronic center of mass energy. $f_{H_k,i}(x_k)$ are the (unrenormalized) *parton distribution functions* (PDFs). They describe the probability of finding a parton i with momentum fraction x_k inside the hadron H_k. Lorentz invariance of the partonic cross section allowed us to conclude that it can only depend on the partonic center of mass energy $\hat{s}$

$$\mathrm{d}\hat{\sigma}_{ij\to n}(x_1 P_1, x_2 P_2, \mu_R) = \mathrm{d}\hat{\sigma}_{ij\to n}(x_1 x_2 S, \mu_R). \tag{2.36}$$

We then defined the *partonic luminosity*

$$\mathcal{L}_{ij}(\tau) \equiv (\tilde{f}_{H_1,i} \otimes \tilde{f}_{H_2,j})(\tau) \equiv \int_0^1 \mathrm{d}x_1 \mathrm{d}x_2\, \tilde{f}_{H_1,i}(x_1) \tilde{f}_{H_2,j}(x_2) \delta(\tau - x_1 x_2), \tag{2.37}$$

where $\tilde{f}_{H,i}(x) \equiv x f_{H,i}(x)$, to arrive at the second line of Eq. (2.35).

At this stage the partonic cross section can still exhibit singularities whenever a finial state parton becomes collinear to one of the initial state partons. At LO for example, the divergence due to initial-state collinear emissions reads

$$\mathrm{d}\hat{\sigma}_{ab\to cX}(s, \mu_R)\Big|_{\text{div.}} = -\frac{\alpha_s}{2\pi}\frac{1}{\epsilon} \int_0^1 \mathrm{d}z\, \left(P_{db}^{(0)}(z) \mathrm{d}\hat{\sigma}_{ad\to X}(zs, \mu_R) + P_{da}^{(0)}(z) \hat{\sigma}_{db\to X}(zs, \mu_R) \right), \tag{2.38}$$

where $P_{ij}^{(0)}$ are the LO *Altarelli-Parisi splitting kernels*[7]:

$$\begin{aligned} P_{qq}^{(0)}(x) &= C_F \left[\frac{1+x^2}{(1-x)_+} + \frac{3}{2}\delta(1-x) \right], \\ P_{qg}^{(0)}(x) &= T_F \left[x^2 + (1-x)^2 \right], \\ P_{gq}^{(0)}(x) &= C_F \left[\frac{1+(1-x)^2}{x} \right], \\ P_{gg}^{(0)}(x) &= 2C_A \left[\frac{x}{(1-x)_+} + \frac{1-x}{x} + x(1-x) \right] + \delta(1-x)\frac{\beta_0}{2}. \end{aligned} \tag{2.39}$$

7 The definition of β_0 can be found in Eq. (4.49)

We absorb these collinear singularities into the PDFs through a process called *collinear renormalization*, by defining the renormalized PDFs $f_{H,i}(x,\mu_F)$ via

$$f_{H,i}(x) \equiv (Z_{ij}(\cdot,\mu_F) \otimes f_{H,j}(\cdot,\mu_F))(x). \tag{2.40}$$

Beyond the pole term, the renormalization constants are generally scheme dependent. From Eq. (2.38) we see that the $\overline{\text{MS}}$ renormalization constant at NLO are given by

$$Z_{ij}(z,\mu_R,\mu_F) = \delta(1-z)\delta_{ij} + \frac{\alpha_s}{2\pi}\frac{1}{\epsilon}P^{(0)}_{ij}(z) + \mathcal{O}\big(\alpha_s^2\big)\,. \tag{2.41}$$

Now the sum

$$\mathrm{d}\sigma_{H_1H_2\to cX} + \mathrm{d}\sigma_{H_1H_2\to X} \tag{2.42}$$

is guaranteed to be free initial-state collinear divergences.

Since the initial state collinear divergences are of a completely different origin than the UV divergences, we introduce a new scale μ_F, called the factorization scale. This scale separates the long-distance (non-perturbative) physics, contained in the PDFs, from the short-distance (perturbative) physics, contained in the partonic cross sections.

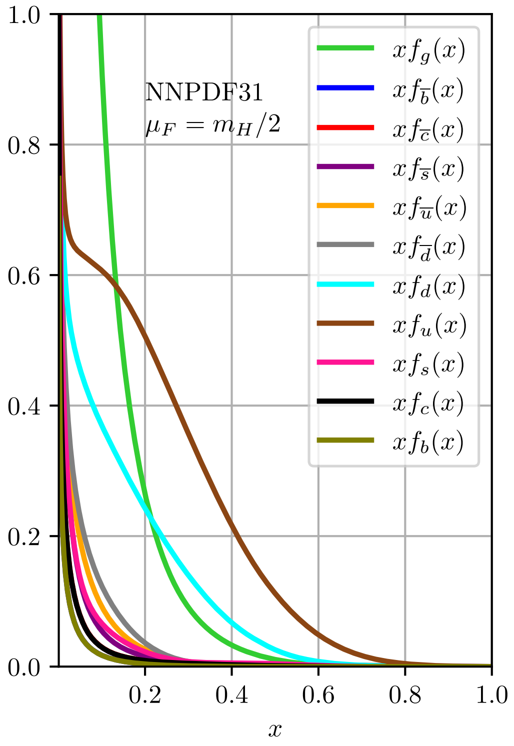

Figure 2.2: The various PDFs multiplied by x as a function of x. The plot was created using the `LHAPDF6` [9] interface to the `NNPDF31_nnlo_as_0118` [10] PDF set at a scale of $\mu_F = m_H/2$.

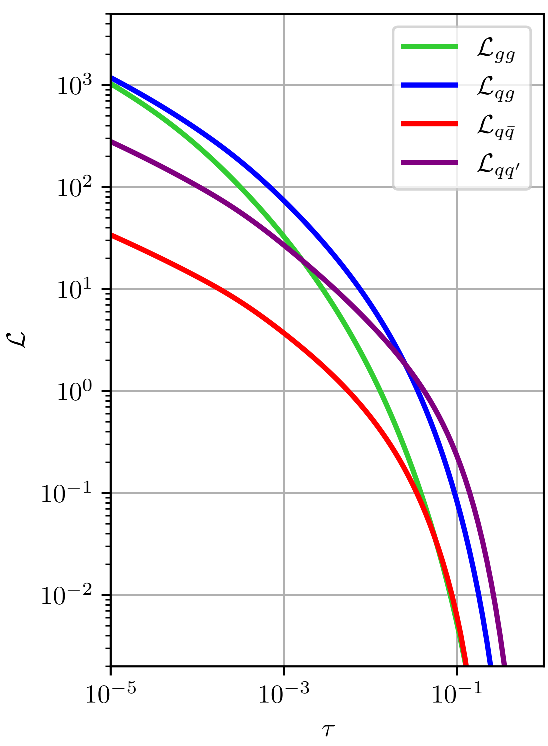

Figure 2.3: Displayed is the partonic luminosity for combinations of various partons. The luminosities are defined as $\mathcal{L}_{qg} = 2\times\sum_i(\mathcal{L}_{q_ig}+\mathcal{L}_{\bar{q}_ig})$, $\mathcal{L}_{q\bar{q}} = 2\times\sum_i \mathcal{L}_{q_i\bar{q}_i}$, $\mathcal{L}_{qq'} = \sum_{i,j}(\mathcal{L}_{q_iq_j}+\mathcal{L}_{q_i\bar{q}_j}+\mathcal{L}_{\bar{q}_i\bar{q}_j})-\mathcal{L}_{q\bar{q}}$. The setup is the same as in Fig. 2.2.

The factorization theorem (2.35) is central in the SM as it tells us that the PDFs are universal quantities, i.e. they are not specific to any one process. It is a postulate of the parton model, in which hadrons are thought of as collection of the free elementary particles. In QCD however, the theorem requires proof [11]! The PDF for all light partons are displayed in Fig. 2.2. In Fig. 2.3 we show the partonic luminosity for exemplary parton combinations. PDFs describe long range interactions, a regime in which QCD is non-perturbative. As such, PDFs are non-perturbative objects which have to be measured in experiments or be calculated non-pertubatively, e.g. on the lattice.

The factorization scale in unphysical in the sense that it is not a parameter in our theory, nor can it be measured in an experiment. As usual we can apply the RGE to determine the running of the renormalized PDFs

$$0 = \frac{\mathrm{d}}{\mathrm{d}\ln\mu_F} f_{H,i}(x) = \frac{\mathrm{d}}{\mathrm{d}\ln\mu_F}(Z_{ij} \otimes f_{H,j}(\cdot,\mu_F))(x). \tag{2.43}$$

This can be rewritten to

$$\begin{aligned}\frac{\mathrm{d}f_{H,i}(x,\mu_F)}{\mathrm{d}\ln\mu_F} &= 2\alpha_s \left(Z^{-1}_{ij} \otimes \frac{\mathrm{d}Z^{(1)}_{jk}}{\mathrm{d}\alpha_s} \otimes f_{H,k}(\cdot,\mu_F) \right)(x,\mu_F) \\ &= \frac{\alpha_s}{\pi}\left(P^{(0)}_{ij} \otimes f_{H,j}(\cdot,\mu_F)\right)(x) + \mathcal{O}\left(\alpha_s^2\right),\end{aligned} \tag{2.44}$$

where $Z^{(1)}_{ij}$ is the residue of the renormalization constant. So even though the PDFs are non-perturbative, their dependence on the factorization scale is. Eq. (2.44) is the famous *Dokshitzter-Gribow-Lipatow-Altarelli-Parisi-evolution equation* (DGLAP equations) [12, 13, 14].

In the derivation above, we have treated the partons inside the hadrons as massless, which leads to real collinear singularities. In reality, all quarks have finite masses, so the phase-space integration only yields logarithmic mass enhancements of the form $\ln(\hat{s}/m_q^2)$ instead of actual singularities. The DGLAP equations then automatically resum these logarithms. For most applications at the LHC, the typical hard scattering scale is orders of magnitudes larger than all quark masses except for the top quark mass. It is therefore beneficial to treat them as massless partons, as the appearance of the large logarithms would otherwise completely destroy the perturbative convergence. However, treating quarks as massless also implies that we neglect their mass-dependent effects in the hard-scattering matrix elements. If the scattering process is sensitive to the quark masses—for example, in processes involving Higgs couplings to quarks—these mass effects might be lost.

The number of quark flavors treated as active (massless) partons defines our *flavor scheme* (FS). For instance, if we treat the lightest four flavors (up, down, strange, charm) as massless, while considering the bottom and top quarks as massive, we are working in the 4FS. Analogously, if the bottom quark is also considered massless, we are working in the 5FS, and so on.

2.2.3 The Phase-Space Integration

Even after renormalization and collinear renormalization can the amplitude exhibit divergences. The scatting amplitude in and of itself is not a physical observable; therefore, it is not required to be finite. Physical observables are cross sections, which are obtained by performing phase-space integrations over the squared amplitudes. However, even after integrating over the phase space, the cross section is not guaranteed to be finite. The reason is that the Born process is indistinguishable from processes with additional infrared radiation. Indeed, no matter how precise a detector is, below a certain resolution, it becomes impossible to detect a very soft photon or to distinguish two highly collinear jets. Hence, computing a cross section with a fixed final state does not make physical sense. Instead, one must consider sufficiently inclusive observables—so called *IR-safe observables*. For these, Kinoshita, Lee and Nauenberg proved that in unitary theories all IR singularities cancel [15, 16]. This is known as the Kinoshita-Lee-Nauenberg (KLN) theorem.

An example of an observable which is trivially IR safe is the fully inclusive cross section

$$\hat{\sigma}_{ij\to n+X} = \sum_{k=1}^{\infty} \hat{\sigma}_{ij\to n+k}, \quad \text{for} \quad \hat{\sigma}^{(0)}_{ij\to n} \quad \text{finite}, \tag{2.45}$$

where $n+k$ indicates that in addition to the final state n we now have k massless partons of whatever flavor. In perturbation theory, the infinite sum is truncated at a given order and at each order

$$\hat{\sigma}^{(l)}_{ij\to n+X} = \sum_{k=0}^{l} \hat{\sigma}^{(l-k)}_{ij\to n+k}, \tag{2.46}$$

summed together with the contribution from collinear renormalization will be finite. For example at NLO, the finite inclusive cross section reads

$$\hat{\sigma}^{(1)}_{ij\to n+X} = \hat{\sigma}^{R}_{ij\to n} + \hat{\sigma}^{V}_{ij\to n} + \hat{\sigma}^{C}_{ij\to n}, \tag{2.47}$$

where

$$\hat{\sigma}^{R}_{ij\to n} = \frac{1}{F}\int \mathrm{d}\Phi_{n+1} \sum_{c} |M^{(0)}_{ij\to n+c}|^2 \tag{2.48}$$

is the real correction,

$$\hat{\sigma}^{V}_{ij\to n} = \frac{1}{F}\int \mathrm{d}\Phi_{n}\, 2\mathrm{Re}\left(\left(M^{(0)}_{ij\to n}\right)^{*} M^{(1)}_{ij\to n}\right) \tag{2.49}$$

is the virtual correction, and

$$\hat{\sigma}^{C}_{ij\to n} = \frac{1}{F}\int \mathrm{d}\Phi_{n}\, \frac{\alpha_s}{2\pi}\frac{1}{\epsilon}\left(\frac{\mu_R^2}{\mu_F^2}\right)^{\epsilon} \sum_{c}\int_0^1 \mathrm{d}z\, \left[P^{(0)}_{ci}(z)|M^{(0)}_{cj\to n}|^2 + P^{(0)}_{cj}(z)|M^{(0)}_{ic\to n}|^2\right] \tag{2.50}$$

are the corrections from collinear renormalization. Figure 2.4 provides a pictorial representation of the required partonic cross sections for Higgs boson production in the gluon fusion channel at various perturbative orders.

Although the sum of the contributions to the cross section is guaranteed to be finite due to the KLN theorem, the presence of IR singularities in individual terms poses significant challenges for practical calculations. These singularities prevent a straightforward evaluation of the phase-space integrals. To overcome this, we once again have to introduce regulators (such as dimensional regularization) to make the integrals well-defined. Over the years, numerous techniques have been developed to compute phase-space integrals efficiently. These techniques can generally be categorized into two main types: *Analytic methods*, and *numerical methods*.

As the name suggests, in the former class, the phase-space integrals are solved analytically. One noteworthy member of this class is the *reverse-unitarity method* [17], which was first applied to Higgs production in the gluon fusion channel. The method uses unitarity, to rewrite the phase-space integrals in terms of loop integrals over cut-propagators. One can then apply the remarkable techniques developed for Feynman integrals to these phase-space integrals and

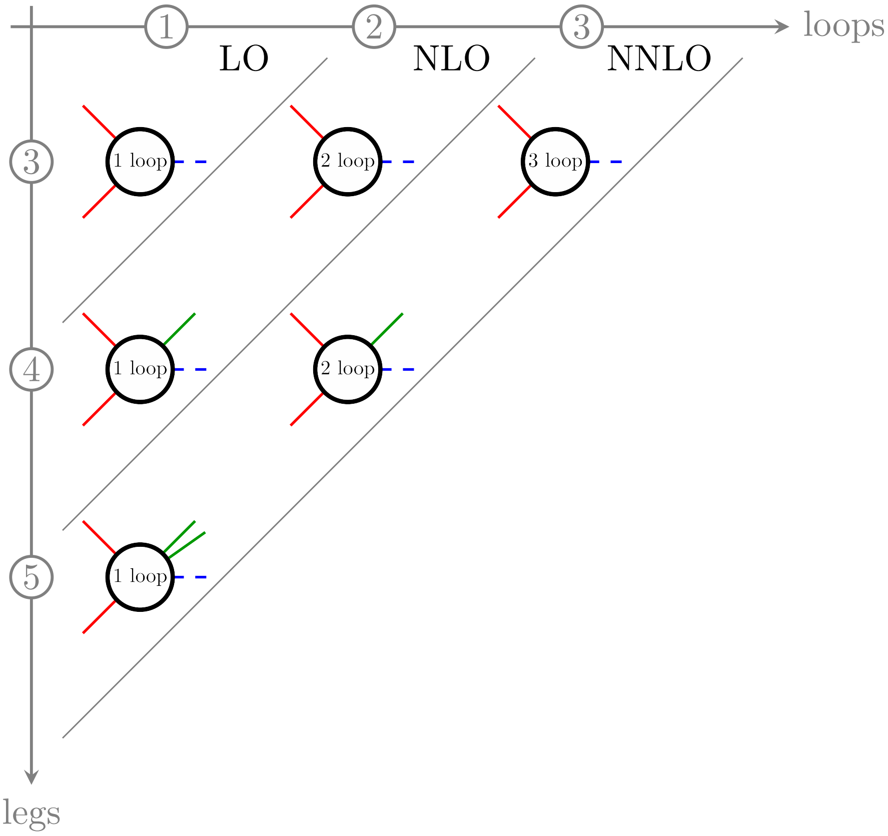

Figure 2.4: Pictorial representation of the needed partonic cross sections at various perturbative orders of the fully inclusive hadronic cross section. The graphic shows the example of Higgs production in the gluon fusion channel.

solve them analytically. The mayor downside of this approach is that it is highly process and observable dependent, meaning that for every process and every observable we have to start over from scratch. Furthermore, by the very nature of the method, you are always restricted to inclusive jet observables. Nevertheless, it has been successfully applied to, among others, Higgs-rapidity and Higgs-p_T distributions [18].

Among the numerical methods, there are two mayor approaches: *slicing* and *subtraction methods*. The former rely on a variable that isolates the IR-sensitive region of the phase space. Consider once again the example of Higgs production. Here, the IR-sensitive region of the phase space corresponds to configurations where the transverse momentum of the Higgs boson, p_T, approaches zero. The phase-space integral can then be decomposed into

$$\int_0^{p_T} \mathrm{d}k_T \, \mathrm{d}\hat{\sigma}_{ij\to H+c} = \int_0^{p_T^{\mathrm{cut}}} \mathrm{d}k_T \, \mathrm{d}\hat{\sigma}_{ij\to H+c} + \int_{p_T^{\mathrm{cut}}}^{p_T} \mathrm{d}k_T \, \mathrm{d}\hat{\sigma}_{ij\to H+c}. \tag{2.51}$$

The first integral on the right-hand side is now finite and can be computed numerically, e.g. using *Monte-Carlo* (MC) techniques. If we choose p_T^{Cut} small enough, then we can approximate the integrand in the second integral, by its IR limit and solve the integral analytically. The pole of the integral should then cancel against the poles in the virtual integration and the counter term from collinear renormalization. The mayor advantage of this method is its simplicity. One big downside is its dependence on the unphysical cutoff scale. Ideally it is chosen very small, such that the approximation introduces little to no error. But if chosen too small, the integrations will have huge logarithmic enhancements which can easily spoil the numerical precision. Another disadvantage is that not all processes or observables have easily identifiable slicing variables, or the analytic integration is very challenging. For example, p_T slicing only works for color singlet production, indeed if we have a jet in the final state, we can encounter collinear divergences also at finite transverse momenta of the jet. For processes involving jets, a possible slicing variable is the N-jettiness

$$\mathcal{T}_N \equiv \sum_k \min_i \left\{ \frac{2p_i \cdot q_k}{Q_i} \right\}, \tag{2.52}$$

with N, the number of jets, q_k, the momenta of the unresolved partons, p_i, the momenta of the resolved jets, and Q_i a normalization factor which can for example be set to the jet energy. However, the analytic integration becomes highly non-trivial and is a matter of active research. Currently, the N-jettiness beam functions are known at N^{3}LO [19], the 0-jettiness soft function is known at N^{3}LO [20, 21] and NNLO 1-jettiness soft functions and jet functions are also known [22, 23, 24, 25].

Subtraction methods on the other hand, work by subtracting the infrared limits at the integrand level. In the *Frixione-Kunszt-Signer subtraction scheme* (FKS subtraction scheme) one first isolates the IR divergence by partitioning the phase space into *sectors* using *selector functions*. These functions isolate specific infrared limits by approaching unity when a particular limit is approached (e.g., when an unresolved parton becomes soft or collinear) and vanish in other limits. For a single unresolved parton, a possible selector function is

$$\mathcal{S}_{n+1,k} \equiv \frac{1}{d_{n+1,k}} \left(\sum_k \frac{1}{d_{n+1,k}} \right)^{-1}, \quad \text{where} \quad d_{n+1,k} \equiv \left(\frac{E_{n+1}}{\sqrt{\hat{s}}} \right)^{\alpha} (1 - \cos\theta_{n+1,k})^{\beta}. \tag{2.53}$$

The first index $n+1$ is the index of the unresolved parton, while the second index is the index of the reference parton. E_{n+1} denotes the energy of the unresolved parton, this factor is therefore to identify soft singularities. Consequently, the power α can be set to zero if the unresolved parton is a quark. Other than that, the powers must be strictly positive $\alpha, \beta > 0$. If $n+1$ now becomes collinear to one of the partons, say parton i, then the selector function $S_{n+1,i}$ will approach one. And since the selector functions are strictly positive and form a decomposition of unity

$$\sum_k \mathcal{S}_{n+1,k} = 1, \tag{2.54}$$

all other selector functions will go to zero simultaneously.

The real emission cross section can then be written as a sum over sectors:

$$\hat{\sigma}_{ij\to n+u} = \frac{1}{F} \sum_k \int \mathrm{d}\Phi_{n+1} \, |M^{(0)}_{ij\to n+u}|^2 \mathcal{S}_{n+1,k}. \tag{2.55}$$

Now say we found a way to factorize the phase space, such that the infrared limits of a specific sector, are isolated (see for example Ref. [26]). Then in each sector, we will have two unit integrations over ξ and η which parameterize the soft and collinear limit respectively, i.e. if $\xi \to 0$, then the momentum of the unresolved parton goes to zero and if $\eta \to 0$, the unresolved parton will become collinear to the reference momentum of that sector. The amplitude has the singular scaling $|M^{(0)}_{ij\to n+u}|^2 \sim \xi^{-2}\eta^{-1}$, leading to an integral of the form

$$\int_0^1 \frac{\mathrm{d}\eta}{\eta^{1+\epsilon}} \frac{\mathrm{d}\xi}{\xi^{1+2\epsilon}} f(\eta, \xi, \cdots), \tag{2.56}$$

where f is a function regular in the limits $\eta, \xi \to 0$. If we now apply the distributional identity

$$\frac{1}{x^{1-\epsilon}} = \frac{1}{\epsilon}\delta(x) + \sum_{k=0} \frac{\epsilon^k}{k!} \left(\frac{\ln^k x}{x} \right)_+ , \tag{2.57}$$

we can explicitly carry out all integrations.

The *sector improved residue subtraction scheme* [27] extends the FKS subtraction scheme to NNLO. As of today, it is the only subtraction scheme capable of computing any QCD phase-space integral. Beyond NNLO, developing efficient and general subtraction schemes remains an open challenge in perturbative QCD.

3 THE HIGGS AS A WINDOW TO NEW PHYSICS

3.1 STABILITY OF THE HIGGS POTENTIAL

3.2 THE HIERARCHY PROBLEM

4 HADRONIC HIGGS PRODUCTION

4.1 MOTIVATION (BETTER TITLE NEEDED!)

Here I list various application for the Higgs production cross section and explain why precise predictions are so central. Maybe just put this in the chapter description?

4.2 THE LEADING-ORDER CROSS SECTION

Having established, that the gluon-fusion Higgs production cross section is central for many phenomenological applications, we now want to perform the actual LO calculation, which was first demonstrated by Georgi et al. in 1978 [28]. The calculation not only serves as an instructive example on cross section calculation, and thereby allows us to put our experience from section 2.2 to good use, but it already introduces many important concepts we can transfer to the NNLO computation.

At LO, there are only two possible Feynman diagrams we can draw. They are depicted in Fig. 4.1. As we can see. Gluon-fusion is a loop induced process with two scales: the mass of

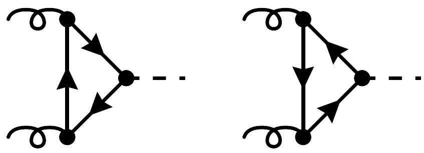

Figure 4.1: LO Feynman diagrams for Higgs production in the gluon-fusion channel.

the quark running in the loop m_q, and the Higgs mass m_H which must simultaneously be the partonic center of mass energy. The initial state gluons carry on the on-shell momenta p_1 and p_2. Let us then define

$$i\mathcal{M} = i\mathcal{M}^{\mu\nu,ab}\varepsilon^a_\mu(p_1)\varepsilon^b_\nu(p_2). \tag{4.1}$$

With the Feynman rules presented in appendix A we find

$$\begin{aligned} i\mathcal{M}^{\mu\nu,ab} &= -\int \frac{\mathrm{d}^4k}{(2\pi)^4} \\ &\times \mathrm{Tr}\left[\frac{-im_q}{v}\delta_{ij}\frac{i(\not{k}+\not{p}_1+\not{p}_2+m_q)}{(k+p_1+p_2)^2-m_q^2}(ig\gamma^\nu T^a_{ik})\frac{i(\not{k}+\not{p}_1+m_q)}{(k+p_1)^2-m_q^2}(ig\gamma^\mu T^b_{kj})\frac{i(\not{k}+m_q)}{k^2-m_q^2}\right] \\ &+ \{p_1 \longleftrightarrow p_2, \mu \longleftrightarrow \nu, a \longleftrightarrow b\}, \end{aligned} \tag{4.2}$$

where the extra minus sign in front stems from the fermion trace.

Even without performing the explicit calculation can we already anticipate the general structure of the amplitude. Color wise, the amplitude must be proportional to δ^{ab}, because it is the only available rank-two tensor. Since it is symmetric, the Lorentz structure must also be symmetric in order to satisfy *Bose symmetry*. The only building blocks we have available are $g^{\mu\nu}$, $(p_1^\mu p_2^\nu + p_2^\mu p_1^\nu)$, $p_1^\mu p_1^\nu$, and $p_2^\mu p_2^\nu$, but since all transverse parts drop out of the physical amplitude, the relevant tensors are only $g^{\mu\nu}$ and $p_2^\mu p_1^\nu$. Lastly, we know that the amplitude must satisfy the *Ward identity*, which allows us to restrict the tensor even further, such that we end up with

$$i\mathcal{M}^{\mu\nu,ab} = i\frac{\alpha_s}{\pi}\frac{1}{v}\delta^{ab}\left(p_2^\mu p_1^\nu - (p_1\cdot p_2)g^{\mu\nu}\right)\mathcal{C}(m_H, m_q). \tag{4.3}$$

Notice that we have only made use of very general properties of the amplitude. This is why the decomposition in Eq. (4.3) will hold at every order of α_s. The function $\mathcal{C}(m_H, m_q)$ is called the *Higgs-gluon form factor*. It has mass dimension 0, i.e. its functional dependence on m_q and m_H must be through a mass ratio

$$\mathcal{C}(m_H, m_q) = \mathcal{C}(z), \quad \text{with} \quad z \equiv \frac{m_H^2}{4m_q^2}. \tag{4.4}$$

The factor of 1/4 was introduced, so that the *normal threshold* is located at $z = 1$. Mathematically, this means that $z = 1$ is a solution of the *Landau equations*. Physically, we can interpret the singularity as the point where we have enough energy to produce the quark pair on-shell. We can now project onto the form factor with

$$\mathcal{C}(z) = \frac{\pi v}{i\alpha_s}\frac{1}{N_c^2-1}\delta^{ab}\frac{1}{(p_1\cdot p_2)^2(d-2)}\left(p_{2\,\mu}p_{1\,\nu} - (p_1\cdot p_2)g_{\mu\nu}\right)i\mathcal{M}^{\mu\nu,ab}. \tag{4.5}$$

Let us define the pertubative expansion of the Higgs-gluon form factor as

$$\mathcal{C} = \mathcal{C}^{(0)} + \frac{\alpha_s}{\pi}\mathcal{C}^{(1)} + \left(\frac{\alpha_s}{\pi}\right)\mathcal{C}^{(2)} + \cdots \tag{4.6}$$

If we now insert the LO expression of Eq. (4.2) and perform some basic manipulations we find for the leading coefficient

$$\begin{aligned}\mathcal{C}^{(0)}(z) = T_F\frac{1}{2-2\epsilon}\frac{1}{z}\int\frac{\mathrm{d}^d k}{i\pi^{d/2}}&\frac{1}{[k^2-m_q^2+i0^+][(k+p_1+p_2)^2-m_q^2+i0^+]}\\ &\times\left(2\epsilon + \frac{m_H^2}{[(k+p_1)^2-m_q^2+i0^+]}\left(\frac{1}{z}+\epsilon-1\right)\right),\end{aligned} \tag{4.7}$$

which, after inserting integrals and expanding in ϵ, finally reduces to

$$\mathcal{C}^{(0)}(z) = T_F\frac{1}{z}\left\{1 - \left(1-\frac{1}{z}\right)\left[\frac{1}{2}\ln\left(\frac{\sqrt{1-1/z}-1}{\sqrt{1-1/z}+1}\right)\right]^2\right\}. \tag{4.8}$$

We see that the Higgs-gluon form factor is roughly proportional to the square of the mass of the quark running in the loop. One power of m_q is hereby picked up from the Yukawa coupling. The other factor m_q is a consequence of the scalar coupling to Higgs. Indeed, without the quark mass, the trace in Eq. (4.2) would contain an odd number of gamma matrices and vanish consequently. Physically, we can interpret this as a helicity flip of the internal quark at the Higgs interaction vertex. And since massless QCD conserves helicity, the other helicity flip is provided by the mass. Similarly, since the two incoming gluons are vector bosons which should form a spinless final state, we would expect them to always carry opposite spins. This intuition is indeed confirmed by the tensor structure of the amplitude (4.3), as it always vanishes once contracted with two polarization vectors of the same helicity[1].

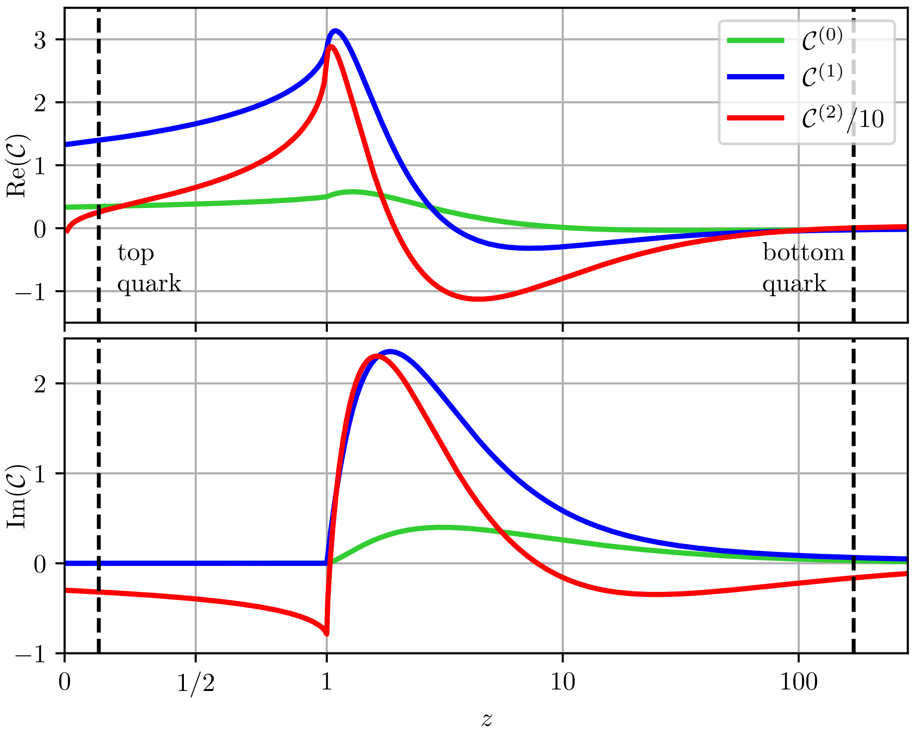

Figure 4.2: Real and imaginary part of the finite part of the Higgs-gluon form factor at various perturbative. NNLO is divided by ten for better visibility. NNLO results also depend on the number of light quark flavors, which has been set to 5 (5FS). Top-quark is renormalized in the OS scheme. Infrared divergences are subtracted in the $\overline{\text{MS}}$ scheme with the help of the **Z** operator (see e.g. Ref. [29]). Vertical lines indicate the z values for the top and bottom quark masses. The plot was created using the results of Ref. [30].

The LO Higgs-gluon form factor is plotted in Fig. 4.2. As expected, we pick up an imaginary part starting from the normal threshold at $z = 1$. If we expand the form factor around large quark masses, i.e. we perform a *large mass expansion* (LME), we find that it approaches a constant

$$\mathcal{C}^{(0)}(z) = T_F \left(\frac{2}{3} + \frac{7}{45} z + \frac{4}{63} z^2 + \mathcal{O}(z^3) \right) . \tag{4.9}$$

We will discuss the infinite mass limit in more detail in section 4.3. On the other side of the spectrum we can see that if the mass of the Higgs is far greater than the mass the internal quark, the form factor is approximately

$$\mathcal{C}^{(0)}(z) = \frac{T_F}{4z} \left[4 - \log^2(-4z) + \frac{1}{z} \left(\log(-4z) + \log^2(-4z) \right) + \mathcal{O}(1/z^2) \right] . \tag{4.10}$$

This expansion is known as *high-energy limit* HEL. The appearing double logarithms $\log^2(m_q^2/m_H^2)$ originate from a soft quark exchange. In fact, the quark mass acts as an infrared regulator of the integral in Eq. 4.7, so the appearance of these logarithms is not entirely unexpected. Numerically, these logarithms can be very large. The bottom quark, for example will yield a double logarithm of about 46. I.e., although suppressed by a factor of m_q^2/m_H^2, the contributions from lighter quark flavors are logarithmically enhanced and hence highly significant for precision predictions.

1 This can be seen easily by boosting to the center of mass frame and using $\epsilon^\mu(-\mathbf{p}, \lambda) \propto \epsilon^\mu(\mathbf{p}, -\lambda)$.

If we now apply Eq. (2.25) and perform the phase space integration, which for a single particle is trivial because of the momentum conserving delta function, we get for the partonic cross section

$$\hat{\sigma}_{gg\to H}(\tau S) = \frac{\pi}{64v^2} m_H^2 \left(\frac{\alpha_s}{\pi}\right)^2 |\mathcal{C}(z)|^2 \delta\big(\tau S - m_H^2\big) \frac{1}{1-\epsilon}. \tag{4.11}$$

The initial state was averaged over spin and color. In conventional dimensional regularization, the gluons have $d-2 = 2(1-\epsilon)$ spin degrees. Finally, after the convolution with the partonic luminosity we arrive at the LO cross section

$$\sigma_{ggH}^{\mathrm{LO}}(S) = \frac{\pi}{64v^2} \left(\frac{\alpha_s}{\pi}\right)^2 \mathcal{L}_{gg}\left(\frac{m_H^2}{S}\right) |\mathcal{C}^{(0)}(z)|^2. \tag{4.12}$$

From Fig. 4.2 we can see that the top quark exerts the largest impact on the Higgs-gluon form factor and hence the LO hadron cross section. We can read off the partonic luminosity from Fig. 2.3 and find that the cross section for the top quark induces Higgs production reads[2]

$$\sigma_{ggH}^{\mathrm{LO}}(t) = 16.30 \text{ GeV} \tag{4.13}$$

at a hadronic center of mass energy of 13 TeV. Although expected to have little impact, we can also include the effects of finite bottom quark masses by coherently summing together the corresponding form factors. We find

$$\sigma_{ggH}^{\mathrm{LO}}(t+b) = 14.72 \text{ GeV}, \tag{4.14}$$

i.e. the bottom quark lowers the cross section by around 9% at LO.

Without the inclusion of electro-weak corrections, we can always decompose the gluon fusion cross section in terms of the Yukawa couplings Y_i:

$$\sigma_{ggH} = \sum_{i\le j} Y_i Y_j \sigma_{ij}. \tag{4.15}$$

We call

$$\sigma_{i\times j} = Y_i Y_j \sigma_{ij}, \tag{4.16}$$

the *i-j-interference contribution* and

$$\sigma_i = Y_i^2 \sigma_{ii} \tag{4.17}$$

the *pure-i contribution* to the cross section. Both contributions are depicted at LO in Fig. 4.3. Clearly, the dominant contribution for the lighter quark flavors comes from the interference with the top-quark. The pure-bottom contribution is already below a percent and the pure-charm quark mass effects are completely negligible. The inclusion of the charm quark lowers the total cross section by around 2%, making it relevant for high precision predictions.

4.3 THE HEAVY-TOP LIMIT

The computation of the Higgs production cross section in full QCD is quite challenging. As we saw above, even at leading order we encounter loop integrals with two mass scales. It is therefore maybe not surprising that the first NLO corrections to this process were actually computed in an approximation framework [31]. In the approximation, we assume that the

2 Values of masses and coupling constants are provided in the conventions.

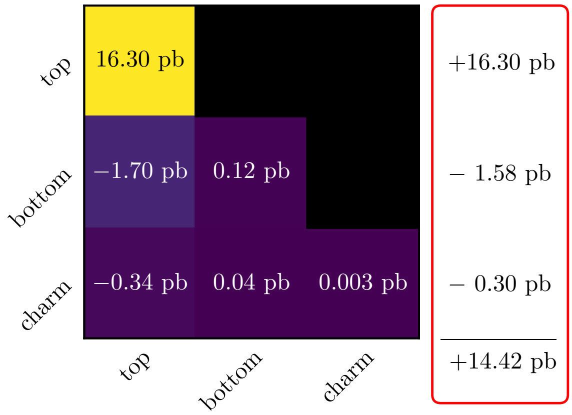

Figure 4.3: σ_i (diagonals) and $\sigma_{i\times j}$ (off-diagonals) at LO for the three heaviest quark flavors. The red box indicates the sum of each row, and hence the combined effects of each additional flavor. The computational setup is described in the conventions.

quark, which is coupling to the Higgs is infinitely heavy. That means we are only interested in the leading term of the LME.

The finite distance interaction of the gluon and the Higgs will therefore shrink down to a point like vertex, which we can describe with the effective Lagrangian

$$\mathcal{L}^{(0)}_{\mathrm{HTL}} = \mathcal{L}^{(n_f-1)}_{\mathrm{QCD}} - C_1 \frac{H}{v}\frac{1}{4} G^a_{\mu\nu} G^{a\,\mu\nu}. \tag{4.18}$$

We see that the coupling constant now has mass dimension -1, so the theory will not be UV renormalizable. That means that we cannot absorb all UV divergences into multiplicative renormalization constants as we did for the SM (see Eq. (2.31)), but we will generate more and more independent terms in our Lagrangian to cancel all appearing divergences. On the other hand, as long as we restrict ourselves to QCD corrections, and hence only single operator insertions, we can treat the color singlet Higgs as a constant, and renormalize only the gauge invariant operator

$$\mathcal{O}_1 \equiv -1/4 G^a_{\mu\nu} G^{a\,\mu\nu}. \tag{4.19}$$

To indicate the pertubative order we gave the Lagrangian in Eq. (4.18) a superscript. The superscript $n_f - 1$ of the QCD Lagrangian specifies the number of active flavors. It was reduced by one, since the heaviest quark flavor was integrated out. The constant C_1 is called a *Wilson coefficient*, and it needs to be matched to the full theory in the infinite quark mass limit. At LO for example, we find that the Higgs-gluon form factor in the effective theory simply reads

$$C_1 = -\frac{\alpha_s}{\pi}\mathcal{C}^{(0)} + \mathcal{O}\big(\alpha_s^2\big)\,. \tag{4.20}$$

If we compare this to the leading term of our LME (4.9), we find

$$C_1 = -\frac{\alpha_s}{\pi}\frac{2}{3}T_F + \mathcal{O}\big(\alpha_s^2\big)\,. \tag{4.21}$$

The main benefit of the approximation lies in the reduced complexity. By integrating out the top quark, we have reduced a loop-induced process to a tree-level process. Moreover, the top-quark mass is eliminated as a scale, hence the appearing Feynman integrals will generally be much simpler to solve.

4.3.1 Renormalization of Gauge Invariant Operators

Beyond LO gauge invariant operator like $\mathcal{O}_1$ can mix under renormalization with other gauge invariant operators but notably also with operators which are not gauge invariant. In general, we distinguish two types of operators: *Type-II operators*, which give zero when sandwiched between physical states, and *type-I operators*, which can give non-zero matrix elements. The type-II operators can be further subcategorized into operators vanishing by the equation of motion (*type-II$_a$ operators*), and all other operators (*type-II$_b$ operators*). For a polynomial operator with ghost number zero satisfying

$$s\mathcal{O} = 0, \tag{4.22}$$

where s is the *linearized Slavnov operator*, one can proof [32, 33, 34] that

$$\mathcal{O} = sF + \text{gauge invariant operators.} \tag{4.23}$$

Operators of the form sF are also called *Bechi-Rouet-Stora-Tyutin-* (BRST-) *exact operators*, and they vanish between physical states. For $\mathcal{O}_1$ the above conditions are met, allowing us to conclude that the $\mathcal{O}_{II}$ operators are BRST-exact. This can be leveraged to find the complete operator basis:

$$\begin{aligned}
\mathcal{O}_I &\begin{cases} \mathcal{O}_1 = -\frac{1}{4} G^a_{\mu\nu} G^{a\,\mu\nu}, \\ \mathcal{O}_2 = \sum_{i=1}^{n_l} m_i \bar{q}_i q_i, \end{cases} \\
\mathcal{O}_{II_a} &\begin{cases} \mathcal{O}_3 = \sum_{i=1}^{n_l} \bar{q}_i \left(\frac{i}{2} \overleftrightarrow{\not{D}} - m \right) q_i, \end{cases} \\
\mathcal{O}_{II_b} &\begin{cases} \mathcal{O}_4 = A^{a\,\mu} D^\nu G^a_{\nu\mu} + g \sum_{i=1}^{n_l} \bar{q}_i \not{A} q_i - \partial^\mu \bar{c}^a \partial_\mu c^a, \\ \mathcal{O}_5 = D_\mu \partial^\mu \bar{c}^a c^a. \end{cases}
\end{aligned} \tag{4.24}$$

The operator basis is constructed only of light fields, and the light fields are defined in a decoupled theory.

Since operators of type II cannot generate non-vanishing S-matrix elements through renormalization the renormalization matrix must have the general structure

$$\begin{pmatrix} \mathcal{O}_I^R \\ \mathcal{O}_{II}^R \end{pmatrix} = \begin{pmatrix} z^{I,I} & z^{I,II} \\ 0 & z^{II,II} \end{pmatrix} \begin{pmatrix} \mathcal{O}_I^B \\ \mathcal{O}_{II}^B \end{pmatrix}. \tag{4.25}$$

The final form of our effective Lagrangian therefore reads

$$\mathcal{L}_{\text{HTL}} = \mathcal{L}^{(5)}_{\text{QCD}} + \frac{H}{v} \sum_{i=1}^{5} C_i^B \mathcal{O}_i^B. \tag{4.26}$$

As usual, we replace the bare quantities by their renormalized counter parts

$$C_i^B \mathcal{O}_i^B = C_i^B Z_{ij}^{-1} \mathcal{O}_j^R, \tag{4.27}$$

and we identify

$$C^R = (Z^{-1})^T C^B. \tag{4.28}$$

Using the RGE we find that the *anomalous dimension* matrix of the Wilson coefficients is determined through

$$\frac{\mathrm{d}C^R}{\mathrm{d}\ln\mu} = \left(Z\frac{\mathrm{d}(Z^{-1})}{\mathrm{d}\ln\mu}\right)^T C^R = -\left(\frac{\mathrm{d}Z}{\mathrm{d}\ln\mu}Z^{-1}\right)^T \equiv \gamma^T C^R. \tag{4.29}$$

With the structure of the renormalization matrix (4.25), we arrive at an important conclusion: The Wilson coefficients of type-II operators cannot mix into the Wilson coefficients of type-I operators through the running in the scale. Since the type-II operators render no contribution to the scattering matrix element, we can focus our attention on the gauge invariant operators and their Wilson coefficients.

We now want to determine the I, I part of the renormalization matrix, i.e. $z^{I,I}$ to determine the running of the Wilson coefficients. Let us start by defining the generating functional

$$\begin{gathered} Z[J] \equiv z[J]/z[0], \quad z[J] \equiv \int \prod_i \mathcal{D}\Phi_j\, e^{i(S+J\cdot\Phi)}, \quad S = S[A, c, \bar{c}, q, \bar{q}] \equiv \int \mathrm{d}^d x\, \mathcal{L}, \\ J = \left(J^\mu, \bar{J}, J, \bar{\eta}, \eta\right), \quad \Phi = \left(\frac{1}{g}A_\mu, c, \bar{c}, q, \bar{q}\right), \end{gathered} \tag{4.30}$$

with the Lagrangian

$$\mathcal{L} \equiv -\frac{1}{4g^2}F^a_{\mu\nu}F^{a\,\mu\nu} - \frac{1}{2\xi g^2}\left(\partial\cdot A\right)^2 + \partial^\mu\bar{c}^a D_\mu c^a + \bar{q}\left(\frac{i}{2}\overleftrightarrow{\not{D}} - m_q\right)q. \tag{4.31}$$

The Lagrangian is the QCD Lagrangian with only one active quark flavor and rescaled gauge fields

$$A^a_\mu \longrightarrow \frac{1}{g}A^a_\mu. \tag{4.32}$$

The operators in Eq. (4.24) can now be generated by applying the differential operators[3]

$$\begin{aligned} D_1 &= -\frac{1}{2}g\frac{\partial}{\partial g} + \xi\frac{\partial}{\partial\xi} - \frac{1}{2}J_\mu\cdot\frac{\delta}{\delta J_\mu}, \\ D_2 &= -m_q\frac{\partial}{\partial m_q}, \end{aligned} \tag{4.33}$$

on the generating functional

$$z_{\mathcal{O}_k}[J] \equiv \int \prod_j \mathcal{D}\Phi_j\, \hat{\mathcal{O}}_k(0) e^{i(S+J\cdot\Phi)} = -iD_k z[J]. \tag{4.34}$$

Here $\hat{\mathcal{O}}_k(0)$ is the Fourier transform of the operator $\mathcal{O}(x)$ at zero momentum. The normalization of the generating functional then properly subtracts the vacuum expectation value of the operators

$$-iD_k Z[J] = \frac{1}{z[0]}\int\prod_j \mathcal{D}\Phi_j\,\left(\hat{\mathcal{O}}_k(0) - \langle\Omega|\mathcal{O}_k(0)|\Omega\rangle\right)e^{i(S+J\cdot\Phi)} \equiv Z_{\mathcal{O}_k}. \tag{4.35}$$

In the $\overline{\mathrm{MS}}$ scheme, the R-operation commutes with the differential operators in Eq. (4.33), i.e. the renormalized operators can be generated from the renormalized generating functional

$$Z_{\mathcal{O}^R_k} = -iD_k Z^R[J], \tag{4.36}$$

3 We only provide the operators for the type-I operators, since they are the only ones necessary for computing physical amplitudes.

where the renormalized generating functional is defined as

$$
\begin{aligned}
Z^R[J] &= z^R[J]/z^R[0], \\
z^R[J] &= \int \prod_i \mathcal{D}\Phi_j \, e^{i(S^R + J\cdot\Phi)}, \\
S^R \equiv S[Z_3'^{1/2} A^R, Z_3'^{-1/2} c^R, &\tilde{Z}_3^{-1/2} \bar{c}^R, Z_2^{1/2} q^R, Z_2^{1/2} \bar{q}^R, Z_g g, Z_m m_q, Z_g^{-2} Z_3' \xi^R].
\end{aligned}
\tag{4.37}
$$

Using the chain rule we find that

$$
-iD_k z^R[J] = \int \prod_j \mathcal{D}\Phi_j \left[\hat{O}_k(0) + \sum_i (D_k \ln Z_i) \frac{\partial S^R}{\partial \ln Z_i} \right] e^{iS^R + J\cdot\Phi}, \quad Z_i \in \{Z_3', \tilde{Z}_3, Z_2, Z_g, Z_m\}.
\tag{4.38}
$$

And with

$$
Z_g \frac{\partial S^R}{\partial Z_g} = -2\hat{\mathcal{O}}_1(0), \quad \text{and} \quad Z_m \frac{\partial S^R}{\partial Z_m} = -\hat{\mathcal{O}}_2(0),
\tag{4.39}
$$

we find that the renormalization constants are given by

$$
\begin{aligned}
z_{11}^{I,I} &= 1 - 2D_1 \ln Z_g = 1 + g\frac{\partial \ln Z_g}{\partial g}, & z_{12}^{I,I} &= -D_1 \ln Z_m = \frac{g}{2}\frac{\partial \ln Z_m}{\partial g} \\
z_{21}^{I,I} &= 0, & z_{22}^{I,I} &= 1.
\end{aligned}
\tag{4.40}
$$

Here we made use of the fact, that the $\overline{\text{MS}}$-renormalization constants are independent of the quark mass and the gauge parameter. We can rewrite the appearing derivatives in terms of the β-function and the mass-anomalous dimension. Indeed,

$$
\begin{aligned}
\frac{4\pi}{\alpha_s}\bar{\beta} \equiv \frac{\mathrm{d}\ln\alpha_s}{\mathrm{d}\ln\mu} &= -\frac{\mathrm{d}\ln Z_{\alpha_s}}{\mathrm{d}\ln\mu} = -\left(\frac{\partial \ln Z_{\alpha_s}}{\partial \ln\alpha_s}\frac{\mathrm{d}\ln\alpha_s}{\mathrm{d}\ln\mu} + \frac{\partial \ln Z_{\alpha_s}}{\partial \ln\mu}\right) = -\left(\frac{4\pi}{\alpha_s}\bar{\beta}\frac{\partial \ln Z_{\alpha_s}}{\partial \ln\alpha_s} + 2\epsilon\right) \\
\Rightarrow \frac{\partial \ln Z_{\alpha_s}}{\partial \ln\alpha_s} &= g\frac{\partial \ln Z_g}{\partial g} = -1 - 2\epsilon\frac{\alpha_s}{4\pi\bar{\beta}} = -1 + \frac{1}{1 - \frac{\beta}{2\epsilon}\frac{4\pi}{\alpha_s}},
\end{aligned}
\tag{4.41}
$$

where in the last step we used the relation between the d- and four-dimensional β-functions

$$
\bar{\beta} = \beta - 2\epsilon\frac{\alpha_s}{4\pi}.
\tag{4.42}
$$

Similarly, we find

$$
\begin{aligned}
\gamma_m \equiv -\frac{\mathrm{d}\ln m_q}{\mathrm{d}\ln\mu} &= \frac{\mathrm{d}\ln Z_m}{\mathrm{d}\ln\mu} = \frac{\partial \ln Z_m}{\partial \ln\alpha_s}\frac{\partial \ln\alpha_s}{\partial \ln\mu} = \frac{\partial \ln Z_m}{\partial \ln\alpha_s}\frac{4\pi}{\alpha_s}\bar{\beta} \\
\Rightarrow \frac{\partial \ln Z_m}{\partial \ln\alpha_s} &= g\frac{\partial \ln Z_m}{\partial g} = \frac{\alpha_s}{4\pi}\frac{1}{\bar{\beta}}\gamma_m = -\frac{\gamma_m}{2\epsilon}\frac{1}{1 - \frac{\beta}{2\epsilon}\frac{4\pi}{\alpha_s}}
\end{aligned}
\tag{4.43}
$$

Finally, we want to use the above results to calculate the anomalous dimension matrix in Eq. (4.29). The entries of the renormalization constant only depend on scale through the coupling constant, i.e.

$$
\gamma^{I,I} = -\frac{\mathrm{d}z^{I,I}}{\mathrm{d}\ln\mu}(z^{I,I})^{-1}\bigg|_{\epsilon=0} = -\frac{\partial z^{I,I}}{\partial\alpha_s}(z^{I,I})^{-1} 4\pi\bar{\beta}\bigg|_{\epsilon=0} = \frac{\partial z^{I,I\,(1)}}{\partial\alpha_s}2\alpha_s.
\tag{4.44}
$$

Where we used that $z^{I,I}$ consists only of poles in the $\overline{\text{MS}}$ scheme, and once again applied the relation between the β-functions in Eq. (4.42). $z^{I,I\,(1)}$ denotes the residue of the renormalization matrix

$$
z^{I,I} = \mathbb{1} + \sum_{i=1} z^{I,I\,(i)}\epsilon^{-i}.
\tag{4.45}
$$

We then find for the anomalous dimension matrix

$$\gamma^{I,I} = \begin{pmatrix} 4\pi\alpha_s \frac{\mathrm{d}}{\mathrm{d}\alpha_s}\left(\frac{\beta}{\alpha_s}\right) & -\alpha_s \frac{\mathrm{d}\gamma_m}{\mathrm{d}\alpha_s} \\ 0 & 0 \end{pmatrix}. \tag{4.46}$$

The structure of this matrix reveals, that the C_1 Wilson coefficient, which is relevant coefficient for the HTL, is completely independent of the other Wilson coefficients. The RGE for the Wilson coefficient (4.29) can now be written as

$$\frac{\partial C_1}{\partial \alpha_s} 4\pi\beta + \frac{\partial C_1}{\partial \ln \mu} = 4\pi\alpha_s \frac{\mathrm{d}}{\mathrm{d}\alpha_s}\left(\frac{\beta}{\alpha_s}\right) C_1. \tag{4.47}$$

The β-function has the general expansion

$$\beta = \left(\frac{\alpha_s}{4\pi}\right)^2 \sum_{i=0} \beta_i \left(\frac{\alpha_s}{4\pi}\right)^i. \tag{4.48}$$

For example at one-, and two-loop, it can be shown [35, 36, 37, 38, 39, 40]

$$\begin{aligned} \beta_0 &= \frac{11}{3} C_A - \frac{4}{3} T_F n_f, \\ \beta_1 &= \frac{34}{3} C_A^2 - \frac{20}{3} C_A T_F n_f - 4 C_F T_F n_f. \end{aligned} \tag{4.49}$$

We can solve the partial differential equation in Eq. (4.47) perturbatively by proposing the Ansatz

$$\begin{aligned} C_1 = {} & \frac{\alpha_s}{4\pi} C_1^{(0,0)} + \left(\frac{\alpha_s}{4\pi}\right)^2 \left(C_1^{(1,0)} + C_1^{(1,1)} \ln \frac{\mu}{\mu_0}\right) \\ & + \left(\frac{\alpha_s}{4\pi}\right)^3 \left(C_1^{(2,0)} + C_1^{(2,1)} \ln \frac{\mu}{\mu_0} + C_1^{(2,2)} \ln^2 \frac{\mu}{\mu_0}\right) + \cdots . \end{aligned} \tag{4.50}$$

The constants coefficients $C_1^{(i,0)}$ mark the initial conditions; they need to be matched to the full theory in the infinite mass limit. The coefficients of the logarithms on the other hand can be determined through a comparison of coefficients, they read

$$\begin{gathered} C_1^{(1,1)} = 0, \\ C_1^{(2,1)} = C_1^{(0,0)}\beta_1 - C_1^{(1,0)}\beta_0, \quad C_1^{(2,2)} = 0, \\ C_1^{(3,1)} = 2C_1^{(0,0)}\beta_2 - 2C_1^{(2,0)}\beta_0, \quad C_1^{(3,2)} = \beta_0^2 C_1^{(1,0)} - \beta_0\beta_1 C_1^{(0,0)}, \quad C_1^{(3,3)} = 0. \end{gathered} \tag{4.51}$$

It is clear from the structure of the differential equation, that the all coefficients $C_1^{(i,i)}$ are in fact all zero except for $C_1^{(0,0)}$.

4.3.2 Matching of Wilson Coefficients

By expanding the Higgs-gluon form for large quark masses we were able to determine the LO Wilson coefficient. Of course, if we would need the full Higgs-gluon form factor to determine the Wilson coefficient, the HTL would be of little use, since it would not bring any simplifications. Fortunately, the large quark mass limit can already be used at the integrand level using the large mass expansion.

Alternatively, one may find the matching coefficients by means of *low-energy theorems* [41, 42, 43]:

$$-iG^{B\,-1}_{\bar{q}_iq_i,\bar{q}_iq_i}(0)G^{B}_{\mathcal{O}_1,\ldots,\mathcal{O}_n,\bar{q}_iq_i}(p_1,\ldots,p_{n-1},0)\Big|_{\text{connected}} = \frac{\partial}{\partial m_i^B}G^{B}_{\mathcal{O}_1,\ldots,\mathcal{O}_n}(p_1,\ldots,p_{n-1})\Big|_{\text{connected}}. \tag{4.52}$$

Here, $\mathcal{O}_1,\ldots,\mathcal{O}_n$ are local operators and $G_{\mathcal{O}_1,\ldots}\big|_{\text{connected}}$ denotes the momentum space representation of the corresponding conntected Green's functions

$$\begin{aligned}\int\left(\prod_{i=1}^{n}\mathrm{d}^d x_i\, e^{ip_i\cdot x_i}\right)\langle\Omega|T\left[\mathcal{O}_1^B(x_1)\ldots\mathcal{O}_n^B(x_n)\right]|\Omega\rangle\,\Big|_{\text{connected}}&\\ \equiv(2\pi)^d\delta^{(d)}\left(\sum_{i=1}^{n}p_i\right)G^{B}_{\mathcal{O}_1,\ldots,\mathcal{O}_n}(p_1,\ldots,p_{n-1})\Big|_{\text{connected}}&,\end{aligned} \tag{4.53}$$

$|\Omega\rangle$ denotes the vacuum of the interacting theory and T is the *time ordering operator*. The theorem relates the mass derivative of a Green's function with a Green's function of the same operators but with the insertion of $\bar{q}_iq_i$ at zero momentum.

It follows upon application of the *Gell-Mann–Low formula*

$$\begin{aligned}&\frac{\partial}{\partial m_i^B}\langle\Omega|T\left[\mathcal{O}_1^B(x_1)\ldots\mathcal{O}_n^B(x_n)\right]|\Omega\rangle\,\Big|_{\text{connected}}=\\ &\langle 0|T\left[\mathcal{O}^B_{1,I}(x_1)\ldots\mathcal{O}^B_{n,I}(x_n)(-i)\int\mathrm{d}^d x\left(1+\frac{H_I^B(x)}{v}\right)\bar{q}_i^B(x)q_i^B(x)\exp\left(-i\int\mathrm{d}^d z\,\mathcal{H}^B_{\text{int},I}(z)\right)\right]|0\rangle\end{aligned} \tag{4.54}$$

The subscript I indicates interaction picture fields, $|0\rangle$ is the vacuum state, now of the free theory, and $\mathcal{H}_{\text{int}}$ is the interaction part of the *Hamiltonian*. Without the inclusion of electroweak corrections, we can omit the Higgs field in the interaction. This also implies, that all operators $\mathcal{O}_1,\ldots,\mathcal{O}_n$, do not contain any electroweak fields. After switching to momentum space, we immediately arrive at Eq. (4.52). The extra inverse propagator $G^{-1}_{\bar{q}_iq_i,\bar{q}_iq_i}(0)$ was inserted, because the $\bar{q}_iq_i$ operator is considered an external field on the left-hand side of Eq. (4.52) but not in Eq. (4.54).

Since the proof relied on relations on the level of the Lagrangian, the statement is only true for bare amplitudes and Green's functions beyond LO. It can be straightforwardly generalized to include an arbitrary number of massive particles, by simply summing over all massive particles. Lastly, we note that the differential operator does not act on masses in the operators themselves, should they contain any.

We can now apply the low-energy theorem on the gluon self energy. Let us consider first the *amputated* Green's function of two gluons with the insertion of the composite operator $\mathcal{O}_h=\bar{h}^Bh^B$. In momentum space, it reads

$$\begin{aligned}G^{B,ab\,\mu\nu}_{A,A,\mathcal{O}_h}(p,0)\Big|_{\text{amp.}}&=\int\mathrm{d}^d x\,\mathrm{d}^d y\,e^{ip\cdot(x-y)}\langle\Omega|T\left[A^{B,a\mu}(x)A^{B,b\nu}(y)\mathcal{O}_h(0)\right]|\Omega\rangle\,\Big|_{\text{amp.}}\\ &\equiv\delta^{ab}\left[-g^{\mu\nu}p^2G^B_{A,A,\mathcal{O}_h}(p^2)\Big|_{\text{amp.}}+\text{terms proportional to }p^\mu p^\nu\right],\end{aligned} \tag{4.55}$$

where T denotes the time ordering operator and p is the momentum along the gluon line. As discussed in detail above, in the limit of infinite quark mass $m_h^B \to \infty$, the operator $\bar{h}h$ can be written in terms of a linear combination of the operators $\mathcal{O}_1, \ldots, \mathcal{O}_5$

$$\begin{aligned} &G^{B,ab\,\mu\nu}_{A,A,\mathcal{O}_h}(p,0)\Big|_{\text{amp.}} \simeq \\ &\quad -\int \mathrm{d}^d x\, \mathrm{d}^d y\, e^{ip\cdot(x-y)} \langle\Omega| T\left[A^{B,a\mu}(x) A^{B,b\nu}(y) \frac{\alpha_s}{\pi}\frac{1}{m_h^B}\sum_{i=1}^{5} C_i^B \mathcal{O}_i^B(0)\right] |\Omega\rangle\Big|_{\text{amp.}}. \end{aligned} \tag{4.56}$$

The $\simeq$ indicates, that the relation holds only up to power corrections of order $1/m_h^{B\,2}$.

In the $\overline{\text{MS}}$ scheme, the *Appelquist-Carazzone decoupling theorem* [44] does not hold in its naïve sense, i.e. heavy degrees of freedom, do not decouple at low energy. The standard method to circumvent this issue, is by the introduction decoupling constants, which relate quantities at in the decoupled theory (denoted with a superscript (n_l)) with the full high energy theory:

$$\begin{aligned} g^{B,(n_l)} &= \zeta_g^B g^B, \quad m_i^{B,(n_l)} = \zeta_{m_i}^B m_i^B, \quad \xi^{B,(n_l)} - 1 = \zeta_3^B(\zeta^B - 1), \\ q_i^{B,(n_l)} &= \sqrt{\zeta_2^B}\, q_i^B, \quad A_\mu^{B,(n_l),a} = \sqrt{\zeta_3^B}\, A_\mu^{B,a}, \quad c^{B,(n_l),a} = \sqrt{\tilde{\zeta}_3^B}\, c^{B,a}. \end{aligned} \tag{4.57}$$

The relations hold up to power corrections of $1/m_h^2$. The decoupling constants are functions of g^B, m_i^B and the scale μ, but the function arguments are left implicit. The amputated Green's functions then becomes[4]

$$\begin{aligned} &G^{B,ab\,\mu\nu}_{A,A,\mathcal{O}_h}(p,0)\Big|_{\text{amp.}} \simeq \\ &\quad -\zeta_3^B \int \mathrm{d}^d x\, \mathrm{d}^d y\, e^{ip\cdot(x-y)} \langle\Omega| T\left[A^{B,(n_l),a\mu}(x) A^{B,(n_l),b\nu}(y) \frac{\alpha_s}{\pi}\frac{1}{m_h^B}\sum_{i=1}^{5} C_i^B \mathcal{O}_i^B(0)\right] |\Omega\rangle\Big|_{\text{amp.}} \end{aligned} \tag{4.58}$$

At LO in α_s, we will have only contributions from the operators $\mathcal{O}_1$ and $\mathcal{O}_4$, because all other operators would create disconnected contributions

$$\begin{aligned} &G^{B,ab\,\mu\nu}_{A,A,\mathcal{O}_h}(p,0)\Big|_{\text{amp.}} \simeq \\ &\quad -\frac{\alpha_s}{\pi}\frac{1}{m_h^B}\delta^{ab}\left(-g^{\mu\nu}p^2\zeta_3^B\left(C_1^B + 2C_4^B\right) + \mathcal{O}(\alpha_s)\right) + \text{terms proportional to } p^\mu p^\nu. \end{aligned} \tag{4.59}$$

We now set the mass of the light quarks in the QCD Lagrangian to zero; the light quark masses in the definition of the operators in Eq. (4.24) can still be non-vanishing. In the limit of vanishing gluon momentum $p \to 0$, the coefficient of the transverse part does not receive any α_s-corrections in DR, because all appearing Feynman integrals are necessarily scaleless. We have thus shown the all order result

$$G^B_{A,A,\mathcal{O}_h}(0,0)\Big|_{\text{amp.}} \simeq -\frac{\alpha_s}{\pi}\frac{1}{m_h^B}\zeta_3^B\left(C_1^B + 2C_4^B\right). \tag{4.60}$$

By application of the LSZ reduction formula we can rewrite the amputated Green's functions in terms of regular ones, then Eq. (4.52) yields

$$\frac{\alpha_s}{\pi}\left(C_1^B + 2C_4^B\right) = \frac{\partial \ln \zeta_3^B}{\partial \ln m_h^B}. \tag{4.61}$$

4 Keep in mind, that the amputated Green's function is an antilinear functional of the fields.

We can repeat the same analysis for $G_{\bar{c},c,\mathcal{O}_h}(p,0)$ and $G_{\bar{c},c,g,\mathcal{O}_h}(p,p,0)$ and in the limit $p \to 0$ obtain

$$\begin{aligned}\frac{\alpha_s}{\pi}\left(-C_4^B - C_5^B\right) &= \frac{\partial \ln \tilde{\zeta}_3^B}{\partial \ln m_h^B}\\ \frac{\alpha_s}{\pi}\left(-C_5^B\right) &= \frac{\partial}{\partial \ln m_h^B}\ln\left(\tilde{\zeta}_3^B\sqrt{\zeta_3^B}\zeta_g^B\right)\end{aligned} \tag{4.62}$$

Eq. (4.61) and (4.62) form a linear system of equations which we can solve for the Wilson coefficients. The solution for the physical Wilson coefficient reads

$$\frac{\alpha_s}{\pi}C_1^B = -\frac{\partial \ln \zeta_g^{B\,2}}{\partial \ln m_h^B}. \tag{4.63}$$

In the $\overline{\text{MS}}$ scheme, the renormalization constant of the heavy quark mass is independent of the mass, i.e.

$$\frac{\partial}{\partial \ln m_h^B} = \frac{\partial}{\partial \ln m_h}. \tag{4.64}$$

With the renormalization matrix in Eq. (4.40) we can then find the renormalized version of Eq. (4.63)

$$\frac{\alpha_s}{\pi}C_1 = -\frac{\partial \ln \zeta_g^2}{\partial \ln m_h}. \tag{4.65}$$

The decoupling constants are known at two-, three-[45] and four-loop [46, 47] order. Notice that we only require the logarithmic dependence of the decoupling constants to obtain the Wilson coefficients. The logarithmic structure on the other hand may be reconstructed from lower order terms in combination with the β-function and the mass anomalous dimension [43]. The four-loop decoupling constant is therefore sufficient, to match the Wilson coefficient up to N^{4}LO. Here we only provide the Wilson coefficient up to N^{3}LO, as it is the highest order for which full cross section calculations are available at present

$$\begin{aligned}C_1^{(0,0)} &= -\frac{4}{3}\\ C_1^{(1,0)} &= -\frac{44}{3}\\ C_1^{(2,0)} &= -\frac{5554}{27} + \frac{76}{3}\ln\left(\frac{m_h^2}{\mu^2}\right) + n_l\left[\frac{134}{9} + \frac{64}{9}\ln\left(\frac{m_h^2}{\mu^2}\right)\right]\\ C_1^{(3,0)} &= \frac{2892659}{486} - \frac{897943}{108}\zeta(3) + \frac{13864}{27}\ln\left(\frac{m_h^2}{\mu^2}\right) - \frac{836}{3}\ln^2\left(\frac{m_h^2}{\mu^2}\right) - \frac{64}{81}\ln^3\left(\frac{m_h^2}{\mu^2}\right)\\ &\quad + n_l\left[-\frac{40291}{243} + \frac{110779}{162}\zeta(3) + \frac{7040}{81}\ln\left(\frac{m_h^2}{\mu^2}\right) - \frac{184}{3}\ln^2\left(\frac{m_h^2}{\mu^2}\right)\right]\\ &\quad + n_l^2\left[\frac{13730}{729} + \frac{308}{81}\ln\left(\frac{m_h^2}{\mu^2}\right) + \frac{128}{27}\ln^2\left(\frac{m_h^2}{\mu^2}\right)\right].\end{aligned} \tag{4.66}$$

Notice that the decoupling constant ζ_g is a function of $\alpha_s^{(n_l+1)}$, i.e. we must recursively apply the decoupling relations (4.57) to express everything in terms of decoupled quantities. The heavy mass m_h is the $\overline{\text{MS}}$ mass.

4.3.3 Higher-Order Corrections

With the effective theory matched, we are ready to discuss higher order corrections to the Higgs production cross section. In the HTL the cross section was computed up to N^{3}LO in the literature [31, 48, 17, 49]. Here, we will briefly recapitulate the NLO calculation, as it nicely illustrates the methods introduces in section 2.2.

We start with the computation of the hard scattering amplitudes. At NLO we require the one-loop Higgs-gluon form factor, and the tree-level amplitudes for $q\bar{q} \to Hg$, $qg \to Hq$, and $gg \to Hg$.

The careful reader might wonder why we do not have to compute the $q\bar{q} \to H$ amplitude. The reason is, that these amplitudes will be zero to all orders. Indeed, the corresponding amplitude would be of the form

$$\mathcal{M}_{q\bar{q}\to H} = i\frac{\alpha_s}{\pi}\bar{v}(p_2)\left[\cdots\right]u(p_1)\delta_{c_1c_2}\frac{1}{v}\mathcal{C}_{q\bar{q}H}, \tag{4.67}$$

where the dots indicate an a priori unknown number of γ-matrices. But since there is no external vector field, the γ-matrices must be fully contracted. The only available objects to contract a γ-matrix with, are either another γ-matrix, or the momenta p_1 or p_2. Contractions among the γ-matrices can always be reduced by applying the anti-commutation relations provided by the Clifford algebra of the γ-matrices. Afterwards, we are left only with contractions with p_1 or p_2. These on the other hand vanish in Eq. (4.67) because of the equation of motion.

The virtual contributions to the cross sections are obtained by evaluating the Feynman diagrams in Fig. 4.4. The result is the NLO correction to the Higgs-gluon form factor in the HTL and reads

$$\mathcal{C}(0) = \frac{1}{3}\left\{1 + \frac{\alpha_s}{\pi}\left(-\frac{m_H^2 + 0^+}{\mu^2}\right)^{-\epsilon}\left(-\frac{3}{2}\frac{1}{\epsilon^2} + \frac{11}{4} + \frac{\pi^2}{8}\right)\right\} \tag{4.68}$$

Using Eq. (4.11) for the partonic $gg \to H$ cross section, we then find

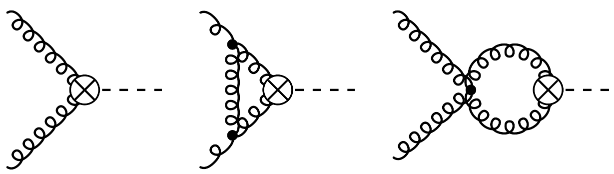

Figure 4.4: One-loop corrections to the Higgs-gluon form factor. The first diagram contributes through the NLO Wilson coefficient.

$$\begin{aligned}\hat{\sigma}_{gg\to H} &= \frac{\pi}{576v^2}\xi\left(\frac{\alpha_s}{\pi}\right)^2\delta(1-\xi) \\ &\times\left[\left(1+\epsilon+\mathcal{O}(\epsilon^2)\right) + \frac{\alpha_s}{\pi}\left(\frac{m_H^2}{\mu^2}\right)^{-\epsilon}\left(-\frac{3}{\epsilon^2} - \frac{3}{\epsilon} + \frac{5}{2} + \frac{7\pi^2}{4} + \mathcal{O}(\epsilon)\right) + \mathcal{O}(\alpha_s^2)\right]\end{aligned} \tag{4.69}$$

where we defined ξ as the of the Higgs mass over the partonic center of mass energy

$$\xi = \frac{m_H^2}{s} = \frac{m_H^2}{\tau S}. \tag{4.70}$$

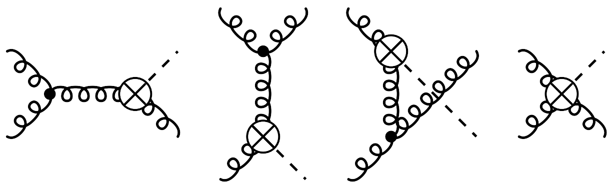

Figure 4.5: Feynman diagrams for the real radiation corrections in the gluon-gluon channel.

As expected, the NLO partonic cross section is not finite on its own, because the IR divergences only cancel in inclusive observables. We must therefore also compute the real radiation corrections as well as the contributions from collinear renormalization. For the former, we evaluate the diagrams in Fig. 4.5 and obtain the averaged squared amplitude

$$\overline{|\mathcal{M}_{gg\to Hg}|^2} = \frac{1}{N_A^2 4(1-\epsilon)^2} \frac{\alpha_s^3}{v^2} \left(\frac{32}{3\pi}\right) \left[(1-2\epsilon)\frac{m_H^8 + s^4 + t^4 + u^4}{stu} + \frac{\epsilon}{2}\frac{\left(m_H^4 + s^2 + t^2 + u^2\right)^2}{stu}\right], \tag{4.71}$$

where N_A is the dimension of the adjoint representation, i.e. $N_A = N^2 - 1$ for SU(N) groups. The symbols s, t and u denote the usual *Mandelstam variables.* Since the Mandelstam variables are not completely independent, as they must satisfy

$$s + t + u = m_H^2, \tag{4.72}$$

the squared matrix element only depends on the final state momenta through t or u. The phase-space integral is $2 * d$ dimensional. We can reduce one of the d dimensional integrals via the momentum conserving delta function. Using spherical coordinates and the remaining two delta functions which ensure on-shellness of the Higgs and the final state gluon, we can carry out the energy and momentum magnitude integral explicitly. This is particularly simple in the center of mass frame. We are hence left with an integral over the $\mathcal{S}_1^{d-2}$ sphere. If we now apply the recursion relation

$$\int_{\mathcal{S}_1^{d-2}} = \int \mathrm{d}\cos\theta \sin^{d-4}\theta \int_{\mathcal{S}_1^{d-3}}, \tag{4.73}$$

and use that the amplitude only depends on the azimuthal angle, i.e. the scattering angle of the Higgs (or gluon), we can carry out the integral over the $\mathcal{S}_1^{d-3}$ sphere explicitly. In the end the phase-space integral is a single one-dimensional integral

$$\text{P.S.} = \frac{1}{8\pi}\frac{1}{\Gamma(1-\epsilon)}\left(\frac{s}{\mu^2 e^{\gamma_E}}\right)^{-\epsilon}(1-\xi)^{1-2\epsilon}\,\Theta(1-\xi)\int_0^1 \mathrm{d}\omega\,\omega^{-\epsilon}(1-\omega)^{-\epsilon}, \tag{4.74}$$

where ω is related to the scattering angle of the Higgs via

$$\omega = \frac{1+\cos\theta}{2}. \tag{4.75}$$

The amplitude in Eq. (4.71) is proportional to $1/tu$, i.e. it diverges if the final state gluon becomes collinear to one of the initial state gluons. Consequently, we expect the appearance of poles once we perform the phase-space integration. Indeed, we find after a straightforward integration

$$\begin{aligned}\hat{\sigma}_{gg\to Hg} &= \frac{1}{576\pi^2}\frac{\alpha_s}{v}(1-\xi)^{-1-2\epsilon}\left(\frac{s}{\mu^2}\right)^{-\epsilon}\Theta(1-\xi) \\ &\times\left[-\frac{3}{\epsilon}\left(1+\xi^4+(1-\xi)^4\right)-\frac{11}{2}(1-\xi)^4-6(1-\xi+\xi^2)^2+\epsilon\left(\frac{3\pi^2}{2}-6+(1-\xi)\cdot(\cdots)\right)\right].\end{aligned} \tag{4.76}$$

The cross section also has a soft singularity at $\xi\to 1$, which can be regulated by applying the distributional identity in Eq. (2.57). The $\mathcal{O}(\epsilon)$ terms proportional to $(1-\xi)$ we only hinted at in Eq. (4.76) will hence not contribute as they are only integrated together with the delta function $\delta(1-\xi)$. The final result then reads

$$\begin{aligned}\hat{\sigma}_{gg\to Hg} = \frac{1}{576\pi^2}\frac{\alpha_s^3}{v^2}\left(\frac{s}{\mu^2}\right)^{-\epsilon}\Theta(1-\xi)\Bigg\{&\left[\frac{3}{\epsilon^2}+\frac{3}{\epsilon}+3-\frac{3\pi^2}{4}\right]\delta(1-\xi) \\ -\frac{6\xi}{\epsilon}&\left[\frac{\xi}{(1-\xi)_+}+\frac{1-\xi}{\xi}+\xi(1-\xi)\right](1+\epsilon)-\frac{11}{2}(1-\xi)^3 \\ +6&\left(\frac{\log(1-\xi)}{1-\xi}\right)_+\left[1+\xi^4+(1-\xi)^4\right]\Bigg\}.\end{aligned} \tag{4.77}$$

The poles proportional to the delta function $\delta(1-\xi)$ exactly cancel between real (4.77) and virtual contributions (4.11). The remaining divergences should cancel after coupling and collinear renormalization. According to Eq. (2.38), the additional contribution from collinear renormalization is

$$\hat{\sigma}^C_{gg\to Hg} = 2\times\frac{\alpha_s}{2\pi}\frac{1}{\epsilon}\int_0^1 \mathrm{d}z\, P^{(0)}_{gg}(z)\hat{\sigma}_{gg\to H}(zs) = \frac{1}{576\pi^2}\frac{\alpha_s^3}{v^2}\frac{1}{\epsilon}\xi P_{gg}(\xi)(1+\epsilon). \tag{4.78}$$

With the definition of the splitting kernel in Eq. (2.39), we see that the remaining poles in the real radiation contribution are indeed canceled. The additional pole introduced by the collinear renormalization is finally canceled by the charge renormalization. Gathering the fruits of our labor, we determined that the inclusive partonic cross section at NLO reads

$$\begin{aligned}\hat{\sigma}_{gg\to HX} &= \frac{\alpha_s^2}{576\pi v^2}\Theta(1-\xi)\Bigg\{\delta(1-\xi) \\ &+\frac{\alpha_s}{\pi}\Bigg[\delta(1-\xi)\left(\pi^2+\frac{11}{2}\right)-\frac{11}{2}(1-\xi)^3+6\left(1+\xi^4+(1-\xi)^4\right)\left(\frac{\log(1-\xi)}{1-\xi}\right)_+ \\ &\qquad+\xi P_{gg}(\xi)\log\left(\frac{s}{\mu^2}\right)\Bigg]\Bigg\}\end{aligned} \tag{4.79}$$

We can carry out the same analysis for the $q\bar{q}$ and qg channel. The Feynman diagrams are depicted in Fig. 4.6. The amplitude for $q\bar{q}\to Hg$ does not exhibit any collinear or soft divergences, rendering collinear renormalization unnecessary. The result for the cross section reads

$$\hat{\sigma}_{q\bar{q}\to Hg} = \frac{1}{486\pi^2}\frac{\alpha_s^3}{v^2}\Theta(1-\xi)\,(1-\xi)^3\,. \tag{4.80}$$

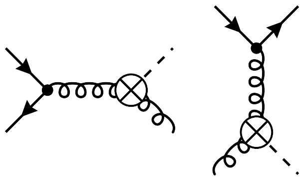

Figure 4.6: Feynman diagrams contributing to the $q\bar{q}$ (left) and qg (right) channel of the Higgs production cross section.

The qg-channel on the other hand has a collinear divergence when the final state quark becomes collinear to the initial state quark. After collinear renormalization we find for the cross section

$$\hat{\sigma}_{qg\to Hg} + \hat{\sigma}^{C}_{qg\to Hg} = \frac{\alpha_s^3}{576\pi^2 v^2}\Theta(1-\xi) \times \left\{(1-\xi)\frac{3\xi-7}{3} + \frac{1}{2}\xi P_{gq}(\xi)\left[1+\log\left(\frac{s}{\mu^2}\right) + 2\log(1-\xi)\right]\right\}. \tag{4.81}$$

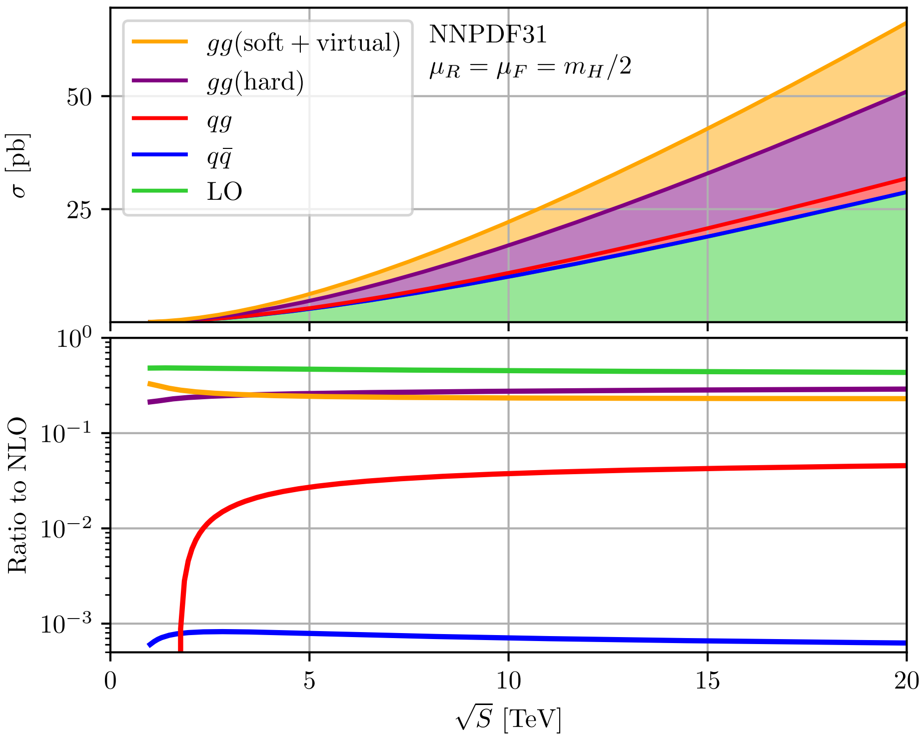

Figure 4.7: Hadronic cross section as function of the hadronic center of mass energy. The total cross section is partinioned into its various channels. The channel denoted "soft + virtual" collects the leading terms of the threshold expansion around $(1-\xi)$ in Eq. (4.79), that is all terms proportional to $\delta(1-\xi)$ and irreducible plus distributions. The lower plot shows the ratio of the various channels to the leading order cross section. Computational setup is described in the conventions.

After convolution of the partonic cross section with the partonic luminosity we get the hadronic cross section, which is displayed in Fig. 4.7 as a function of the hadronic center of mass energy. The cross section is split into the various channels. The "soft + virtual" channel denotes all contributions which originate from integrating the delta function $\delta(1-\xi)$ and irreducible plus distributions, i.e. terms of the form

$$\left(\frac{f(\xi)}{1-\xi}\right)_+ \mathcal{O}\big((1-\xi)^0\big) \tag{4.82}$$

At NLO, it only comes from gluon-induced Higgs production (4.11).

The majority of the hadronic cross section is due to a gluon-gluon initial state, making up more than 95% over the full spectrum of energies. Roughly half of this contribution comes from LO. The other half is composed, yet again of roughly two equal parts, the "soft + virtual" contribution and the remaining real radiation part. The quark-gluon initial state has the second largest impact, whereas the quark-quark induced Higgs production is completely negligible, contributing below 1‰. The large suppression of the $q\bar{q}$ channel is almost entirely due to the reduced partonic luminosity of the channel. Indeed, from Fig. 2.3, we see that the $q\bar{q}$ flux is roughly 30 times smaller than the qg one. This is also the order of magnitude of the ratio of the qg and $q\bar{q}$ induced Higgs production cross section.

The gluon-gluon and quark-gluon luminosity on the other hand is rather similar, especially close to the production threshold, where most of the contributions to the cross section comes from, since larger values are suppressed by $\mathcal{L}/\tau$. Yet we observe that quark-gluon-channel contribution is almost an order of magnitude smaller than in the gluon-gluon channel. To investigate the origin of this suppression, we can look at the coefficient of the logarithm $\log(\mu^2)$ which is predetermined by the RGE

$$\frac{\partial\hat{\sigma}_{qg\to Hq}}{\partial\log\mu^2} = -\frac{\alpha_s}{2\pi}\int_0^1 \mathrm{d}\xi\, P_{gq}(\xi)\hat{\sigma}_{gg\to H}, \quad \frac{\partial\hat{\sigma}_{gg\to Hg}}{\partial\log\mu^2} = -2\times\frac{\alpha_s}{2\pi}\int_0^1 \mathrm{d}\xi\, P_{gg}(\xi)\hat{\sigma}_{gg\to H}. \tag{4.83}$$

At the threshold, the ratio quark-gluon to gluon-gluon logarithmic coefficients is thus $C_F/(4C_A) = 1/9$, which is also roughly the ratio we observed in their contribution to the cross section. The origin of the suppression, is thus partly due to the difference in the color factor and the additional combinatorial factors in the gluon-gluon channel.

Since the NLO corrections are of the same magnitude as the LO cross section, the perturbative result is not yet reliable. One would need to go to even more loops and higher multiplicities in the hope to reach perturbative convergence.

4.3.4 Phenomenological Application

Having discussed the HTL at length, it is important to investigate how well the approximation works for phenomenological applications. In Fig. 4.8, we show the relative error of the cross section in the HTL compared to the results with a finite quark mass for different powers of α_s in the various partonic channels.

At LO, the HTL underestimates the cross section by around 6.5%. In the HTL, the Higgs-gluon form factor, is accurate up to power corrections of order $z = m_H^2/4m_t^2 \approx 13\%$, so the observed accuracy of the approximation aligns with our expectations. For radiative corrections, $m_H^2/m_t^2 \approx 52\%$ is the more natural expansion parameter and the quark-gluon as well as the quark-quark channel show, that they are indeed only roughly 50% accurate.

The gluon-gluon channel on the other hand shows a remarkable property: the accuracy of the HTL stays quite constant across perturbative orders in α_s. In our opinion, this feed is

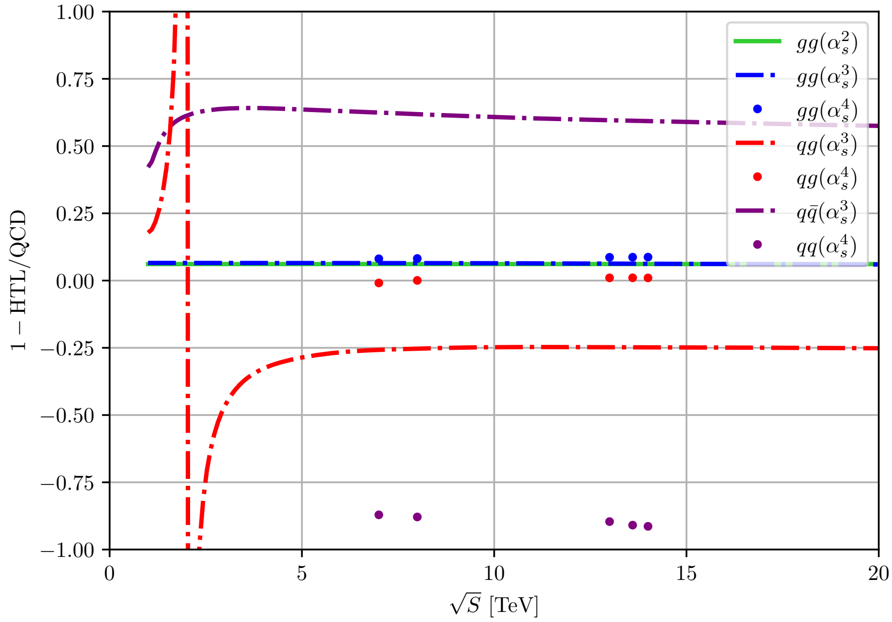

Figure 4.8: Relative error of the HTL compared to the results with finite top-quark mass for various center of mass energies. Displayed are contributions to the cross section in each partonic channels. The computational setup is described in the conventions. The methods to compute the NNLO results with finite top-quark mass are described in chapter 5.

explained by the fact, that much of the structure of the perturbative corrections is dictated by lower orders, and that, for this channel in particular, these kinds of corrections turn out to be numerically large. Indeed, we can apply *Catani's I operator* [50] to predict the poles, as well as the overall factor $(-m_H^2/\mu^2)^{-\epsilon}$, of the Higgs-Gluon form factor in Eq. (4.68). So the part of the partonic cross section which is derived from LO reads

$$\begin{aligned}\hat{\sigma}_{gg\to H}\Big|_{\propto\sigma^{(0)}_{gg\to H}} &= \frac{\pi}{576v^2}\xi\left(\frac{\alpha_s}{\pi}\right)^2\delta(1-\xi)\\ &\times\left[\left(1+\epsilon+\mathcal{O}(\epsilon^2)\right)+\frac{\alpha_s}{\pi}\left(\frac{m_H^2}{\mu^2}\right)^{-\epsilon}\left(-\frac{3}{\epsilon^2}-\frac{3}{\epsilon}-3+\frac{3\pi^2}{2}+\mathcal{O}(\epsilon)\right)+\mathcal{O}(\alpha_s^2)\right].\end{aligned} \tag{4.84}$$

Numerically, the finite part is largely dominated by the π^2 term which originated from the analytic continuation of the Sudakov (double) logarithm. The analytic continuation needed at time-like momentum transfer thus causes a large logarithm. The logarithm on the other hand stems from a soft gluon exchange in the loop.

For the real radiation cross section, we can once again already anticipate initial state collinear as well as the soft divergences

$$\begin{aligned}\hat{\sigma}_{gg\to Hg} &= \frac{1}{576\pi^2}\frac{\alpha_s}{v}(1-\xi)^{-1-2\epsilon}\left(\frac{s}{\mu^2}\right)^{-\epsilon}\Theta(1-\xi)\\ &\times\left[-\frac{1}{\epsilon}\xi(1-\xi)P^{(0)}_{gg}(\xi)\frac{2(-1+2\epsilon)\Gamma(-\epsilon)}{\Gamma(3-2\epsilon)}+(1-\xi)^2\cdot(\cdots)\right].\end{aligned} \tag{4.85}$$

The $(1-\xi)^2$ terms, which we denoted by $(\cdots)$ are finite and regular in the soft limit $\xi\to 1$. We know, that there cannot be any terms of order $(1-\xi)$ apart from those in the splitting function, because every term in the matrix element (4.71) which is constant in the soft limit, still has collinear divergences in the phase-space. I.e. all next to soft contributions are captured in the splitting function. In fact, if we compare with the cross section in Eq. (4.76), then we see that the actual lowest order term is even $(1-\xi)^4$.

The partonic luminosity together with the factor $1/\tau$ cause a strong enhancement of the phase-space region close to the threshold $\xi \to 1$ or $\tau \to m_H^2/S$. Therefore, the hadronic cross section will be well approximated by convoluting the inclusive cross section

$$\begin{aligned}\hat{\sigma}_{gg\to HX}\Big|_{\propto\sigma^{(0)}_{gg\to H}} &= \frac{\alpha_s^2}{576\pi v^2}\Theta(1-\xi)\Bigg\{\delta(1-\xi)\\ &+ \frac{\alpha_s}{\pi}\Bigg[\delta(1-\xi)\pi^2\left(\frac{3}{4}+\mathcal{O}(1/\pi^2)\right)+6\left(1+\xi^4+(1-\xi)^4\right)\left(\frac{\log(1-\xi)}{1-\xi}\right)_+\\ &+\xi P_{gg}(\xi)\log\left(\frac{s}{\mu^2}\right)\Bigg]\Bigg\}.\end{aligned} \tag{4.86}$$

Numerically, we find that the approximation is around 90% accurate at NLO. The main deviations are caused by the soft-virtual channel. We can therefore expect to see deviations in the rescaling factor

$$r^{\mathrm{N}^n\mathrm{LO}} = \frac{\sigma^{\mathrm{QCD,N}^n\mathrm{LO}}_{gg\to HX}}{\sigma^{\mathrm{HTL,N}^n\mathrm{LO}}_{gg\to HX}} \tag{4.87}$$

across perturbative orders of the order of $10\% \times z \approx 1\%$. **TODO:** Add reference to results for finite top-quark masses.

Strictly speaking, our discussion was limited to NLO. However, we claim that most of the arguments are transferable to higher orders in perturbation theory. Indeed, the factor π^2 from analytic continuation can be included to all order by resumming the Sudakov logarithm we encountered [51],i.e. the driving contribution is indeed proportional to the born cross section. This procedure is also sometimes referred to as π^2*-resummmation*. At high orders of perturbation theory, it was demonstated [49], that the quality of the resummation deteriorates, that mean that the Sudakov logarithms are no longer the driving contributor to the soft-virtual contribution. We can therefore expect to see larger deviations from the exact rescling at higher orders. Similarly, our discussion on how to obtain the leading coefficients of the threshold expansion by requiring cancelation of initial-state collinear divergences can also be transferred to higher order [52]. At N^{3}LO, one can correctly predict the three leading logarithms $\log^{5,4,3}(1-\xi)$.

We can leverage the small corrections on the rescaling parameter to improve the HTL cross section results by rescaling the HTL results by

$$\sigma^{\mathrm{rHTL,N}^n\mathrm{LO}}_{gg\to HX} = r^{\mathrm{LO}}\sigma^{\mathrm{HTL,N}^n\mathrm{LO}}_{gg\to HX}, \tag{4.88}$$

where the superscript “rHTL”, now refers to the *rescaled heavy top limit*. Since the gluon-gluon channel is the dominant production channel and the rescaling factor remains quite constant across the perturbative orders, the rHTL cross section will yield a good approximation ($\sim 1\%$) for the Higgs production cross section[5].

5 Excluding the effects from light quark masses.

4.4 THEORY STATUS

Having analyzed the gluon-gluon fusion Higgs production cross section at LO, and NLO in the HTL. We are now equipped with all concepts to discuss state-of-the-art theory predictions.

As already mentioned, the most precise theoretical predictions come from N^{3}LO cross sections in the HTL [53, 49]. They apply the method of reverse unitarity (see section 2.2.3) to perform the phase-space integration fully analytically. The cross section is calculated in terms of a deep expansion in the threshold parameter $(1-\xi)$

$$\hat{\sigma}_{ij\to HX} = \delta_{ig}\delta_{jg}\hat{\sigma}_{\mathrm{SV}} + \sum_{n=0}^{N} c_{ij}^{(n)}(1-\xi)^n, \tag{4.89}$$

where $\hat{\sigma}_{\mathrm{SV}}$ is the leading term, the soft-virtual contribution we already encountered. The soft-virtual contribution has been calculated in Ref. [54]. Because the partonic luminosity is concentrated heavily around the threshold region, one would expect, to see good convergence of the hadronic cross section. Indeed, Ref. [53] computed the first 37 terms of the threshold expansion found that the hadronic cross section is already well approximated by the first five terms.

In the meantime, results without reliance on the threshold expansion have become available [55], confirming the expected accuracy of the threshold expansion and shifting the total cross section by around +0.10 pb at 13 TeV.

In Fig. 4.9 we show the results for the gluon-gluon fusion cross section in the rHTL at various perturbative orders as a function of the hadronic center of mass energy.

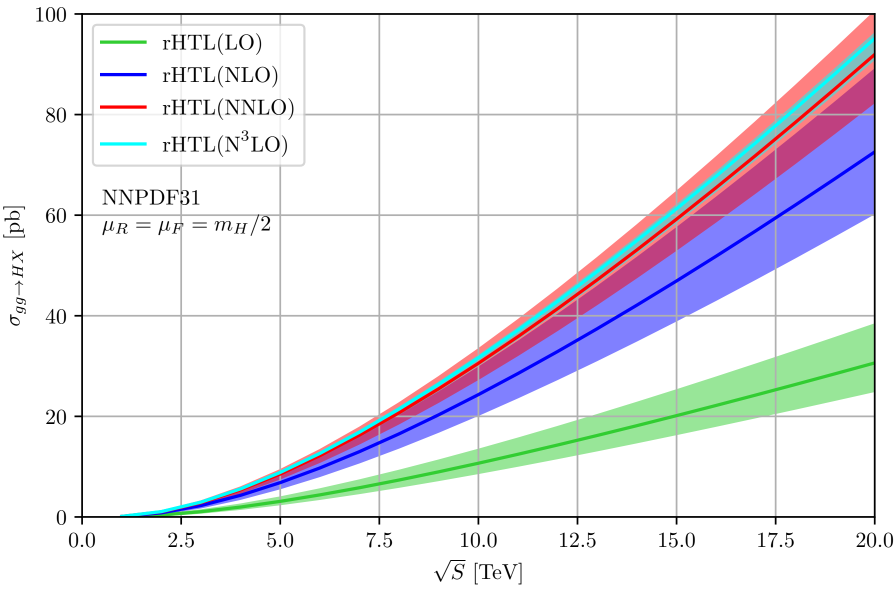

Figure 4.9: Gluon-gluon fusion hadronic cross section as a function of the center of mass energy. Displayed are results computed in the rHTL at various perturbative orders. Transparent bands indicate the scale uncertainty calculated by variation of μ_R in the range $[m_H/4, m_H]$. The computational setup is described in the conventions. The plot was created with the help of `SusHi` [56, 57].

As we discussed before, the NLO cross section is about twice as large as predicted in the Born approximation. NNLO corrections are still sizeable, contribution roughly 20% to the cross section. The NLO scale uncertainties underestimate the effect of higher orders, as the central NNLO cross section is outside the previous uncertainty bands. Only when we go to N^3LO do we see perturbative convergence and corrections consistent with the previous scale uncertainty bands. The scale uncertainties at this order are below 4% for the displayed collision energies.

At this level of precision, it becomes important to investigate other sources of uncertainty and perform a careful evaluation of their impact on the cross section. The most important sources are

- The Scale Uncertainties,
- The PDF uncertainties,
- Uncertainties related to electroweak corrections,
- Uncertainties related to finite top-quark masses,
- Uncertainties related to light quarks.

In the following we will discuss them one-by-one.

4.4.1 Scale Uncertainties

Scale uncertainties serve as an estimate of missing higher order corrections. They are typically computed by 7-point-scale variation, that means the cross section is evaluated at a central scale μ and the additional 6 points $(\mu_R, \mu_F) = (\mu/2, \mu/2), (\mu/2, \mu), (\mu, \mu/2), (2\mu, \mu), (\mu, 2\mu), (2\mu, 2\mu)$. The envelope of the cross section at the seven points then form the scale uncertainty. Since the renormalization and factorization scale is unphysical, physical observables like the cross section are in principle independent of the scales. However, as we are truncating the pertubative series at some fixed order, we are left with some residual dependence of the scale. The scale dependence is therefore a good indicator of missing higher orders. Even so, at low orders the scale uncertainties cannot always be trusted as Fig. 4.9 illustrates nicely.

Fig. 4.10 shows the functional dependence of the hadronc cross section on the renormalization and factorization scale for various perturbative orders. We see that there is very little dependence on the factorization scale, i.e. the vast majority of the scale uncertainties derive from the variation of renormalization scale. This also justifies, why the scale uncertainties in Fig. 4.9 are computed with a fixed factorization scale. We also observe that the dependence on the scale nicely stabilizes as we increase the perturbative precision. For the central scale, $\mu_R = \mu_F = m_H/2$ has become the de facto standard for the inclusive cross section and is also the recommendation of the Higgs working group [58]. The observed functional dependence in Fig. 4.10 supports this choice, as the N^3LO corrections are minor at this scale and the cross section is particularly flat in this regime. It should be noted, that the miniature dependence on the factorization scale is only observed for the total cross section. If instead, we are considering individual production channels, the functional dependence remains very large, because the DGLAP equations mix the quark and gluon PDFs.

The scale uncertainties can be further reduced by including higher order corrections. Although full N^4LO predictions are still beyond the current state-of-the-art in computational capabilities, we can predict at least some parts of the higher order corrections.

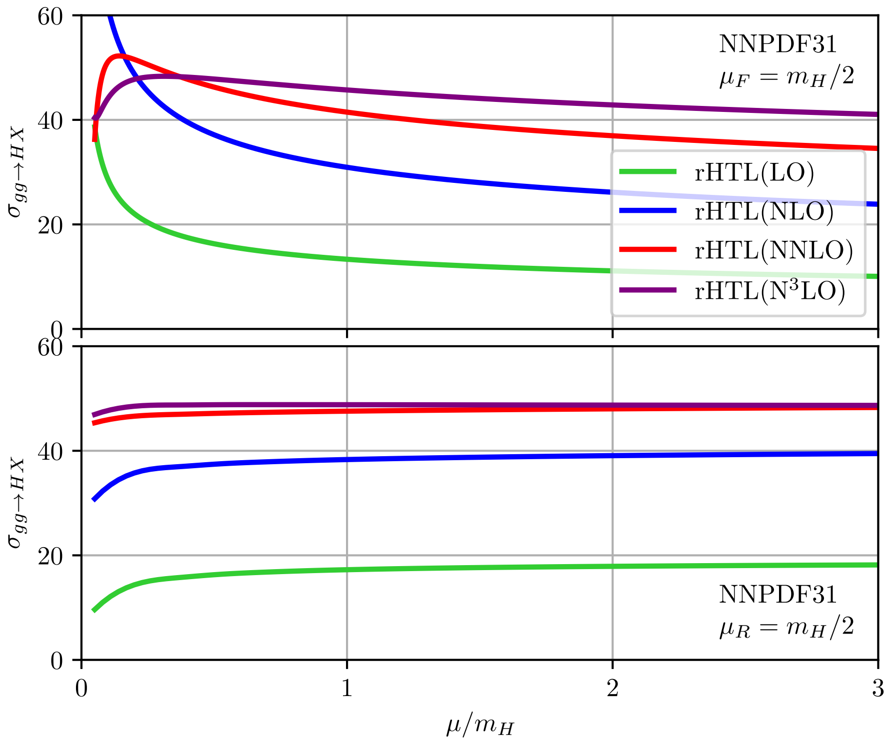

Figure 4.10: Hadronic cross section as a function of the renormalization scale (top panel) and factorization scale (bottom panel). The respective other scale is kept fixed at $m_H/2$. The computational setup is described in the conventions. The plot was created with the help of `SusHi` [56, 57].

Results in the soft-virtual approximation

Since the partonic luminosity is sharply peaked around the threshold (see Fig. 2.3) $\xi \to 1$ or alternatively $\tau \to m_H^2/S$, we can get a good approximation of the hadronic cross section, by expanding the partonic cross section around the threshold as seen in Eq. (4.89). The leading term, i.e. the soft-virtual approximation has been already been computed up to 3 loops [59] in the HTL. Furthermore, as we discussed in section 4.3.4, the cancelation of initial state collinear divergences can be leveraged to determine the leading 3 logarithms of the first subleading term. This means that at N^{4}LO we can predict the coefficients of the logarithms[6]

$$\log^{7,6,5}(1-\xi) \tag{4.90}$$

in $c_{ij}^{(0)}$. This is especially important to stabilize the factorization scale dependence, since otherwise we would introduce an additional contribution to the cross section which is only present in one channel, the gluon-gluon channel, which would scale with running of the PDFs.

At the central scale of $\mu_R = \mu_F = m_H/2$, the partial N^{4}LO results shift the cross section by around -0.1%. Scale uncertainties are reduced from around 4% to below 2.5%. The systematic uncertainty coming from the truncation of the threshold expansion is estimated by comparing the full cross section results with the soft-virtual approximation at lower order, and rescaling the error to the N^{4}LO correction. The error is estimated to be well below 1% of the total cross section. **TODO:** This seems very large. Ask Gotam!

6 In fact one can also get parts of the $\log^4(1-\xi)$ coefficient.

Threshold Resummation
The threshold logarithms appearing in $c_{ij}^{(0)}$ can actually by resummed to all orders. The Hadronic cross section can be cast into the form

$$\sigma(N) = \sum_{ij} f_i(N, \mu_F) f_j(N, \mu_F) \hat{\sigma}_{ij}(N, \mu_R, \mu_F), \tag{4.91}$$

where we switched from τ-space to N-space by means of a *Mellin transform*

$$\sigma(N) = \int_0^1 \mathrm{d}\tau\, \tau^{N-1} \frac{\sigma(\tau)}{\tau}. \tag{4.92}$$

In N-space, also called *Mellin space*, the threshold region $\tau \to m_H^2/S$ corresponds to the limit $N \to \infty$. In this limit, it can be shown [60, 61, 62, 63], that the partonic cross section satisfies the resummed form

$$\hat{\sigma}_{ij}(N) = \delta_{ig}\delta_{jg}\hat{\sigma}^{\mathrm{LO}}_{gg\to H} C_{gg} \exp[\mathcal{G}_H(\log N)] + \mathcal{O}(1/N)\,. \tag{4.93}$$

C_{gg} collects all constant contributions for $N \to \infty$ and can therefore be extracted from lower orders in the large N limit. $\mathcal{G}_H$ contains the threshold logarithms, which get resummed by exponentiation. It requires the cusp anomalous dimension, known today at four-loop accuracy [64], which enables the computation of full N^{3}LO + next-to-next-to-next-to-leading logarithm cross section results. The results[7] [49] show, that at the central scale, the fixed and resummed cross section is nearly identical. This can be interpreted as additional validation of our scale choice. Additionally, it confirms the N^{4}LO soft virtual approximation, which also found that the corrections at the central scale are very close to zero.

π^2-Resummation
In section 4.3.4, we showed that the soft-virtual contribution to the cross section is dominated by a Sudakov logarithm at time-like momentum transfer. This fact can be exploited to predict numerically large coefficients at higher orders and ultimately can be used perform an all order resummation, sometimes referred to as π^2-resummation [51].

Since the logarithm stems from a soft gluon exchange, we can apply techniques from *soft-collinear effective theory* (SCET) [65, 66] to map the Higgs-gluon form factor to a Wilson coefficients of SCET. In SCET we integrate out all the hard modes, such that we can approximate

$$G^a_{\mu\nu} G^{a\,\mu\nu} \longrightarrow C_S(-q^2)(-q^2) g_{\mu\nu} \mathcal{A}^{a\,\mu}_{n\perp} \mathcal{A}^{a\,\nu}_{\bar{n}\perp}, \tag{4.94}$$

where $\mathcal{A}^{\mu\,a}_{n\perp}$ and $\mathcal{A}^{a\,\nu}_{\bar{n}\perp}$ are effective, gauge invariant operators representing gluons traveling along the light-like directions n and $\bar{n}$ defined by the momenta of the incoming hadrons. q^2 is the square of the momentum of the operator and C_S is the Wilson coefficient. The Higgs-gluon form factor in SCET, and hence the leading logarithmic contribution to the full Higgs-gluon form factor is then simply given by **TODO:** Why?

$$\mathcal{C}(0)\Big|_{\mathrm{SCET}} = C_S(-m_H^2 - i0^+), \tag{4.95}$$

which we can use to match the Wilson coefficient

$$C_S(Q^2) = 1 + \frac{\alpha_s}{4\pi} C_A \left(-\ln^2\left(\frac{Q^2}{\mu^2}\right) + \frac{\pi^2}{6} \right). \tag{4.96}$$

7 The authors of that reference use a Padé approximation for the four-loop cusp anomalous dimension, as the full result was still unknown at that point in time. They claim that the approximation is highly accurate.

The key benefit of working in the SCET framework, is that we can now apply RGE methods. Indeed, the Wilson coefficient satisfies the RGE

$$\frac{\mathrm{d}C_S}{\mathrm{d}\ln\mu} = \left[\Gamma^A_{\text{cusp}} \ln\frac{Q^2}{\mu^2} + \gamma^S\right] C_S, \tag{4.97}$$

where Γ^A_{cusp} is the cusp anomalous dimension of Wilson lines with light-like segments in the adjoint representation, and γ_S is the anomalous dimension of the operator. The solution of the differential equation, therefore automatically yields a resummed expression of the Higgs-gluon form factor. The solution can be written in terms of the recursive equation

$$\begin{aligned} &|C_S(-m_H^2)|^2 = U(m_H^2)|C_S(-m_H^2)|^2, \\ \text{with} \qquad &\ln U(m_H^2) = \frac{\alpha_s(m_H^2)}{\pi}\frac{C_A\pi^2}{2}\left\{1 + \frac{\alpha_s(m_H^2)}{4\pi}\left[C_A\left(\frac{67}{9} - \frac{\pi^2}{3}\right) - T_F n_l \frac{20}{9}\right] + \mathcal{O}(\alpha_s^2)\right\}. \end{aligned} \tag{4.98}$$

We see that the leading π^2 term matches our findings in Eq. (4.84).

The resummation drastically improves results at low order of perturbation theory. However, at higher orders, the quality of the resummation deteriorates. This indicates, that at these orders the factors of π^2 are no longer dominant. The procedure should therefore **not** be used to "improve" the N^{3}LO cross sections.

4.4.2 PDF Uncertainties

All results presented so far, where computed using NNLO PDF sets, including all N^{3}LO cross section results. This creates a mismatch between the hard scattering matrix elements and the PDFs, and the cross sections predictions do in fact not entirely have N^{3}LO accuracy. The reason for applying PDF sets at NNLO accuracy is the lack thereof at N^{3}LO.

PDFs are usually fitted to experimental data and then evolved to the desired scale using the DGLAP equation (2.44). To achieve N^{3}LO accuracy, we therefore require

1. hard scattering amplitudes the PDFs can be matched to,
2. and the N^{3}LO splitting functions for the DGLAP evolution.

Regarding the first point, the exact N^{3}LO coefficient function for *deep-inelastic scattering* in the massless limit are known for a long time [67, 68, 69, 70, 71, 72], whereas massive coefficient functions are only available in approximation frameworks [73, 74]. Furthermore, N^{3}LO predictions for charged- and neutral-current *Drell-Yan* production are also available, both for the total [75, 76, 77] and for differential cross sections [78, 79]. These processes are especially valuable for the matching of the PDFs, since there are experimentally very clean.

In Mellin space, the DGLAP equation (2.44) transforms from an integral-differential equation to just a partial differential equation

$$\frac{\partial f_{H,i}}{\partial \log\mu} = -\gamma_{ij}(N, \alpha_s(\mu)) f_{H,j}(N,\mu), \tag{4.99}$$

where $\gamma_{ij}(N,\alpha_s)$ is related to the Mellin transform of the splitting functions

$$\gamma_{ij}(N, \alpha_s(\mu)) = -\frac{\alpha_s}{\mu}\int_0^1 \mathrm{d}x\, x^{N-1} P_{ij}(x, \alpha_s(\mu)). \tag{4.100}$$

Much progress has been made in evaluating specific moments of the splitting functions [80, 81, 82, 83, 84, 85, 86]. Additionally, parts of the splitting functions can be predicted through resummation techniques at low Bjorken-x, a leading logarithmic [87] and next-to-leading logarithmic [88, 89, 90] accuracy. Very recently, all splitting amplitudes were computed fully analytical by Mistlberger et al. [91], these describe the limit of amplitudes in which two of the external partons become collinear. It represents one important ingredient of the splitting kernel.

Although the evolution kernel are not yet fully known, the ingredients we do have can be still be used to at least construct an approximate N^{3}LO PDF set. Results for such PDF sets were recently published by the `MSHT` [92] as well as the `NNPDF` [93] collaboration, which were then combined in Ref. [94]. They use the available data for deep-inelastic scatteing and Drell-Yan production to fit the PDFs. For the running they use (most of) the known Mellin moments of the splitting kernels and smoothly interpolate between them.

In Fig. 4.11 and Tab. 4.1, we compare the gluon-gluon fusion rHTL cross section results at N^{3}LO computed with different approximate N^{3}LO PDF sets. The `NNPDF40_an3lo_as_01180_mhou`

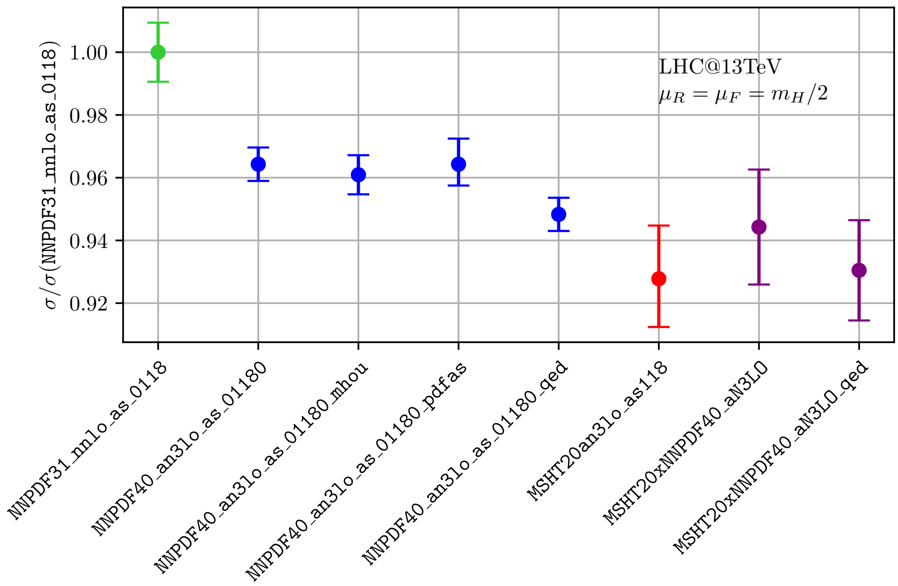

Figure 4.11: Gluon-Gluon fusion cross section in the rHTL at N^{3}LO for various PDF sets normalized by the cross section computed with the `NNPDF31_nnlo_as_0118` PDF set. The provided uncertainties only include the PDF uncertainties. The uncertainty of the normalization is not propagated.

includes *missing higher order uncertainties*. This encompasses the scale uncertainties of the hard scattering matrix elements the PDFs are fitted to, and estimates of the omitted terms in the incomplete N^{3}LO splitting kernels. In the `NNPDF40_an3lo_as_01180_pdfas` PDF set, the replicas are created with different values of α_s between $\alpha_s(m_Z) = 0.117$ and 0.119, in order to estimate the α_s uncertainties. PDF sets ending with "`_qed`", also include corrections from quantum electrodynamics (**qed!**).

Table 4.1: Gluon-Gluon fusion cross section in the rHTL at N^{3}LO for various PDF sets. The provided uncertainties only include the PDF uncertainties.

PDF	$\sigma_{gg\to HX}$ [pb]
NNPDF31_nnlo_as_0118	47.52 ± 0.45
NNPDF40_an3lo_as_01180	45.82 ± 0.25
NNPDF40_an3lo_as_01180_mhou	45.66 ± 0.30
NNPDF40_an3lo_as_01180_pdfas	$45.82^{+0.39}_{-0.32}$
NNPDF40_an3lo_as_01180_qed	45.06 ± 0.25
MSHT20an3lo_as118	$44.09^{+0.81}_{-0.73}$
MSHT20xNNPDF40_aN3LO	44.87 ± 0.87
MSHT20xNNPDF40_aN3LO_qed	44.22 ± 0.76

Before the publication of aN^{3}LO PDF sets, the uncertainty due to the mismatch of the PDF was estimated through lower orders rescaled to N^{3}LO

$$\delta(\mathrm{PDF}-\mathrm{th}) = |\sigma_{gg\to HX}^{\mathrm{NNLO,NNLO\ PDF}} - \sigma_{gg\to HX}^{\mathrm{NNLO,NLO\ PDF}}| \times \left(\frac{\sigma_{gg\to HX}^{\mathrm{N^3LO}}}{\sigma_{gg\to HX}^{\mathrm{NNLO}}} - 1 \right). \tag{4.101}$$

For the `NNPDF31_nnlo_as_0118` PDF set at 13 TeV, this uncertainty turns out to be close to 1%. However, from Fig. 4.11, we can see that with this approach the impact of the N^{3}LO PDFs is severely underestimated, as the results computed with the aN^{3}LOPDFs is shifted by around 4-6%.

We can also see that the different approaches followed by the `NNPDF` and `MSHT` collaboration, yield central values which are not compatible within the uncertainty bands. Furthermore, the PDF-uncertainty estimates differ by almost a factor of 3.

Provided that the provided missing higher order uncertainties are accurate, the approximations of the splitting kernel seems to be very accurate, effecting the cross sections only on the level of 1‰.

The α_s-uncertainties, make up about half of the total PDF uncertainty, as visible from the error increase between the `NNPDF40_an3lo_as_01180` and `NNPDF40_an3lo_as_01180_pdfas` PDF set.

The inclusion of QED effects shifts the cross section by around -0.6 pb at 13 TeV.

4.4.3 Electroweak Corrections

4.4.4 Finite Top-Quark Mass Effects

4.4.5 Effect of Light Quarks

4.4.6 Differential Cross Sections

5 COMPUTATIONAL DETAILS

Description of this chapter.

5.1 COMPUTING THE AMPLITUDES

Here I

5.1.1 The Real-Real Corrections

5.1.2 The Real-Virtual Corrections

5.1.3 The Virtual-Virtual Corrections

5.2 $\overline{\mathrm{MS}}$-SCHEME

5.3 THE 4-FLAVOUR SCHEME

5.4 PERFORMING THE PHASE-SPACE INTEGRATION

6 RESULTS AND DISCUSSION

Description of this chapter.

6.1 TOTAL CROSS SECTION

6.1.1 Effects of Finite Top-Quark Masses

6.1.2 Effects of Finite Bottom-Quark Masses

6.2 DIFFERENTIAL CROSS SECTION

7 CONCLUSIONS

Here are my conclusions.

A | FEYNMAN RULES OF THE STANDARD MODEL

In this chapter we list all Feynman rules of the SM. We choose to work in a unitary gauge, meaning that the all Goldstone-bosons decouple and there are no unphysical particles in the electroweak sector. In the QCD sector, we work in the R_ξ gauge, i.e. we have unphysical particles in the form of *Faddeev-Popov ghosts*. If not otherwise specified, the momenta on every line are defined as incoming.

Propagators:

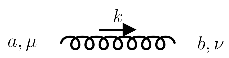

$$= i\frac{\delta^{ab}}{k^2+i0^+}\left[-g_{\mu\nu}+(1-\xi)\frac{k_\mu k_\nu}{k^2+i0^+}\right]$$

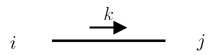

$$= i\delta_{ij}\frac{\not{k}+m}{k^2-m^2+i0^+}$$

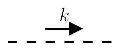

$$= i\frac{1}{k^2-m_H^2+i0^+}$$

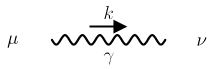

$$= i\frac{-g_{\mu\nu}}{k^2+i0^+}$$

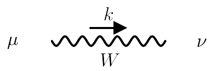

$$= i\frac{1}{k^2-m_W^2+i0^+}\left(-g_{\mu\nu}+\frac{k_\mu k_\nu}{m_W^2+i0^+}\right)$$

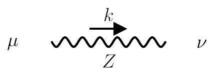

$$= i\frac{1}{k^2-m_Z^2+i0^+}\left(-g_{\mu\nu}+\frac{k_\mu k_\nu}{m_Z^2+i0^+}\right)$$

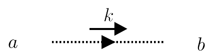

$$= i\frac{\delta^{ab}}{k^2+i0^+}$$

Fermion–Gauge-Boson Vertices:

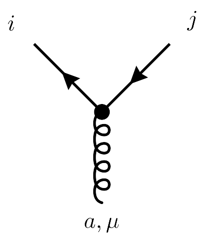

$$= ig\gamma^\mu T^a_{ij}$$

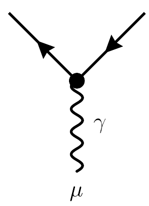

$$= -ie\gamma^\mu Q$$

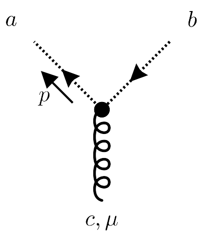

$$= gf^{abc}p^\mu$$

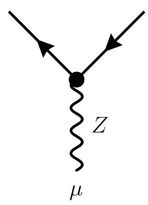

$$= i\frac{e}{\sin\theta_W\cos\theta_W}\gamma^\mu \times \left(I^3 P_L - Q\sin^2\theta_W\right)$$

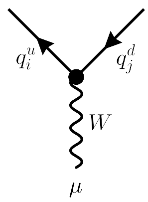

$$= i\frac{e(V_{\mathrm{CKM}})_{ij}}{\sqrt{2}\sin\theta_W}\gamma^\mu P_L$$

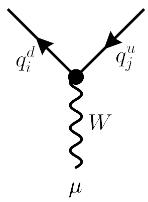

$$= i\frac{e(V_{\mathrm{CKM}})^*_{ji}}{\sqrt{2}\sin\theta_W}\gamma^\mu P_L$$

Gauge-Boson Self Interactions:

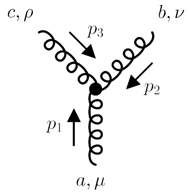

$$\begin{aligned} &= g f^{abc}((p_1^\rho - p_2^\rho)g^{\mu\nu} \\ &\qquad + (p_2^\mu - p_3^\mu)g^{\nu\rho} + (p_3^\nu - p_1^\nu)g^{\rho\mu}) \end{aligned}$$

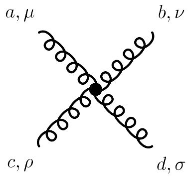

$$\begin{aligned} &= -ig^2\big(f^{abe}f^{cde}(g^{\mu\rho}g^{\nu\sigma} - g^{\mu\sigma}g^{\nu\rho}) \\ &\qquad + f^{ace}f^{bde}(g^{\mu\nu}g^{\rho\sigma} - g^{\mu\sigma}g^{\nu\rho}) \\ &\qquad + f^{ade}f^{bce}(g^{\mu\nu}g^{\rho\sigma} - g^{\mu\rho}g^{\nu\sigma})\big) \end{aligned}$$

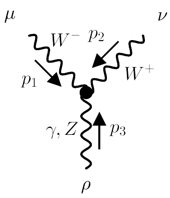

$$\begin{aligned} &= i\tfrac{e}{\sin\theta_W}((p_1^\rho - p_2^\rho)g^{\mu\nu} + (p_2^\mu - p_3^\mu)g^{\nu\rho} \\ &\qquad + (p_3^\nu - p_1^\nu)g^{\rho\mu}) \times \begin{cases} -\sin\theta_W & \text{for } \gamma \\ \cos\theta_W & \text{for } Z \end{cases} \end{aligned}$$

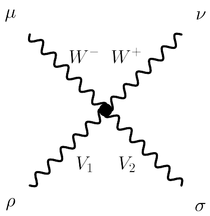

$$= i\frac{e^2}{\sin^2\theta_W}\left(g^{\mu\sigma}g^{\nu\rho} + g^{\mu\rho}g^{\nu\sigma} - 2g^{\mu\nu}g^{\rho\sigma}\right) \times \prod_{i=1}^{2}\begin{cases} -\sin\theta_W & \text{if } V_i = \gamma \\ \cos\theta_W & \text{if } V_i = Z \end{cases}$$

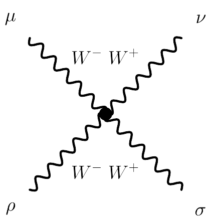

$$= i\frac{e^2}{\sin^2\theta_W}\left(2g^{\mu\rho}g^{\nu\sigma} - g^{\mu\nu}g^{\rho\sigma} - g^{\mu\sigma}g^{\nu\rho}\right)$$

Higgs Interactions:

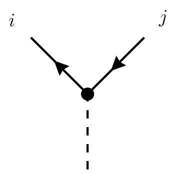

$$= -i\frac{m_q}{v}\delta_{ij}$$

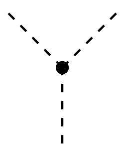

$$= -i\frac{3m_H^2}{v}$$

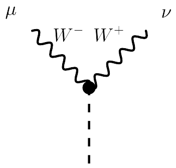

$$= i\frac{e}{\sin\theta_W} m_W g^{\mu\nu}$$

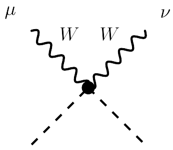

$$= i\frac{e^2}{2\sin^2\theta_W} g^{\mu\nu}$$

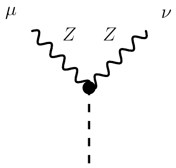

$$= i\frac{e}{\sin\theta_W\cos\theta_W} m_Z g^{\mu\nu}$$

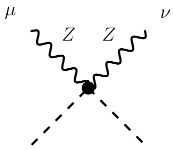

$$= i\frac{e^2}{2\sin^2\theta_W\cos^2\theta_W} g^{\mu\nu}$$

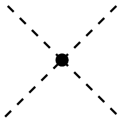

$$= -i\frac{3m_H^2}{v^2}$$

BIBLIOGRAPHY

[1] Michał Czakon, Felix Eschment, and Tom Schellenberger. "Revisiting the double-soft asymptotics of one-loop amplitudes in massless QCD." In: *JHEP* 04 (2023), p. 065. DOI: 10.1007/JHEP04(2023)065. arXiv: 2211.06465 [hep-ph].

[2] Michał Czakon, Felix Eschment, and Tom Schellenberger. "Subleading effects in soft-gluon emission at one-loop in massless QCD." In: *JHEP* 12 (2023), p. 126. DOI: 10.1007/JHEP12(2023)126. arXiv: 2307.02286 [hep-ph].

[3] Michał Czakon et al. "Top-Bottom Interference Contribution to Fully Inclusive Higgs Production." In: *Phys. Rev. Lett.* 132.21 (2024), p. 211902. DOI: 10.1103/PhysRevLett.132.211902. arXiv: 2312.09896 [hep-ph].

[4] Michał Czakon et al. "Quark mass effects in Higgs production." In: *JHEP* 10 (2024), p. 210. DOI: 10.1007/JHEP10(2024)210. arXiv: 2407.12413 [hep-ph].

[5] Izaak Neutelings. *Izaak neutelings.* Mar. 2024. URL: https://tikz.net/sm_particles/.

[6] Stefan Weinzierl. *Feynman Integrals. A Comprehensive Treatment for Students and Researchers.* UNITEXT for Physics. Springer, 2022. ISBN: 978-3-030-99557-7, 978-3-030-99560-7, 978-3-030-99558-4. DOI: 10.1007/978-3-030-99558-4. arXiv: 2201.03593 [hep-th].

[7] Gerard 't Hooft. "Renormalizable Lagrangians for Massive Yang-Mills Fields." In: *Nucl. Phys. B* 35 (1971). Ed. by J. C. Taylor, pp. 167–188. DOI: 10.1016/0550-3213(71)90139-8.

[8] Gerard 't Hooft and M. J. G. Veltman. "Regularization and Renormalization of Gauge Fields." In: *Nucl. Phys. B* 44 (1972), pp. 189–213. DOI: 10.1016/0550-3213(72)90279-9.

[9] Andy Buckley et al. "LHAPDF6: parton density access in the LHC precision era." In: *Eur. Phys. J. C* 75 (2015), p. 132. DOI: 10.1140/epjc/s10052-015-3318-8. arXiv: 1412.7420 [hep-ph].

[10] Richard D. Ball et al. "Parton distributions from high-precision collider data." In: *Eur. Phys. J. C* 77.10 (2017), p. 663. DOI: 10.1140/epjc/s10052-017-5199-5. arXiv: 1706.00428 [hep-ph].

[11] John C. Collins, Davison E. Soper, and George F. Sterman. "Factorization of Hard Processes in QCD." In: *Adv. Ser. Direct. High Energy Phys.* 5 (1989), pp. 1–91. DOI: 10.1142/9789814503266_0001. arXiv: hep-ph/0409313.

[12] Yuri L. Dokshitzer. "Calculation of the Structure Functions for Deep Inelastic Scattering and e+ e- Annihilation by Perturbation Theory in Quantum Chromodynamics." In: *Sov. Phys. JETP* 46 (1977), pp. 641–653.

[13] V. N. Gribov and L. N. Lipatov. "Deep inelastic e p scattering in perturbation theory." In: *Sov. J. Nucl. Phys.* 15 (1972), pp. 438–450.

[14] Guido Altarelli and G. Parisi. "Asymptotic Freedom in Parton Language." In: *Nucl. Phys. B* 126 (1977), pp. 298–318. DOI: 10.1016/0550-3213(77)90384-4.

[15] T. Kinoshita and A. Ukawa. "Mass Singularities of Feynman Amplitudes." In: *Lect. Notes Phys.* 39 (1975). Ed. by Huzihiro Araki, pp. 55–58. DOI: 10.1007/BFb0013300.

[16] T. D. Lee and M. Nauenberg. “Degenerate Systems and Mass Singularities.” In: *Phys. Rev.* 133 (1964). Ed. by G. Feinberg, B1549–B1562. DOI: 10.1103/PhysRev.133.B1549.

[17] Charalampos Anastasiou and Kirill Melnikov. “Higgs boson production at hadron colliders in NNLO QCD.” In: *Nucl. Phys. B* 646 (2002), pp. 220–256. DOI: 10.1016/S0550-3213(02)00837-4. arXiv: hep-ph/0207004.

[18] Falko Dulat et al. “Higgs-differential cross section at NNLO in dimensional regularisation.” In: *JHEP* 07 (2017), p. 017. DOI: 10.1007/JHEP07(2017)017. arXiv: 1704.08220 [hep-ph].

[19] Markus A. Ebert, Bernhard Mistlberger, and Gherardo Vita. “N-jettiness beam functions at N^{3}LO.” In: *JHEP* 09 (2020), p. 143. DOI: 10.1007/JHEP09(2020)143. arXiv: 2006.03056 [hep-ph].

[20] Daniel Baranowski et al. “Zero-jettiness soft function to third order in perturbative QCD.” In: (Sept. 2024). arXiv: 2409.11042 [hep-ph].

[21] Daniel Baranowski et al. “Triple real-emission contribution to the zero-jettiness soft function at N3LO in QCD.” In: (Dec. 2024). arXiv: 2412.14001 [hep-ph].

[22] John M. Campbell et al. “The NNLO QCD soft function for 1-jettiness.” In: *Eur. Phys. J. C* 78.3 (2018), p. 234. DOI: 10.1140/epjc/s10052-018-5732-1. arXiv: 1711.09984 [hep-ph].

[23] Thomas Becher and Guido Bell. “The gluon jet function at two-loop order.” In: *Phys. Lett. B* 695 (2011), pp. 252–258. DOI: 10.1016/j.physletb.2010.11.036. arXiv: 1008.1936 [hep-ph].

[24] Thomas Becher and Matthias Neubert. “Toward a NNLO calculation of the anti-B —> X(s) gamma decay rate with a cut on photon energy. II. Two-loop result for the jet function.” In: *Phys. Lett. B* 637 (2006), pp. 251–259. DOI: 10.1016/j.physletb.2006.04.046. arXiv: hep-ph/0603140.

[25] Radja Boughezal, Xiaohui Liu, and Frank Petriello. “N-jettiness soft function at next-to-next-to-leading order.” In: *Phys. Rev. D* 91.9 (2015), p. 094035. DOI: 10.1103/PhysRevD.91.094035. arXiv: 1504.02540 [hep-ph].

[26] Michał Czakon et al. “Single-jet inclusive rates with exact color at $\mathcal{O}(\alpha_s^4)$.” In: *JHEP* 10 (2019), p. 262. DOI: 10.1007/JHEP10(2019)262. arXiv: 1907.12911 [hep-ph].

[27] M. Czakon. “A novel subtraction scheme for double-real radiation at NNLO.” In: *Phys. Lett. B* 693 (2010), pp. 259–268. DOI: 10.1016/j.physletb.2010.08.036. arXiv: 1005.0274 [hep-ph].

[28] H. M. Georgi et al. “Higgs Bosons from Two Gluon Annihilation in Proton Proton Collisions.” In: *Phys. Rev. Lett.* 40 (1978), p. 692. DOI: 10.1103/PhysRevLett.40.692.

[29] M. Czakon and D. Heymes. “Four-dimensional formulation of the sector-improved residue subtraction scheme.” In: *Nucl. Phys. B* 890 (2014), pp. 152–227. DOI: 10.1016/j.nuclphysb.2014.11.006. arXiv: 1408.2500 [hep-ph].

[30] Micha L. Czakon and Marco Niggetiedt. “Exact quark-mass dependence of the Higgs-gluon form factor at three loops in QCD.” In: *JHEP* 05 (2020), p. 149. DOI: 10.1007/JHEP05(2020)149. arXiv: 2001.03008 [hep-ph].

[31] S. Dawson. “Radiative corrections to Higgs boson production.” In: *Nucl. Phys. B* 359 (1991), pp. 283–300. DOI: 10.1016/0550-3213(91)90061-2.

[32] H. Kluberg-Stern and J. B. Zuber. “Ward Identities and Some Clues to the Renormalization of Gauge Invariant Operators.” In: *Phys. Rev. D* 12 (1975), pp. 467–481. DOI: 10.1103/PhysRevD.12.467.

[33] Satish D. Joglekar and Benjamin W. Lee. “General Theory of Renormalization of Gauge Invariant Operators.” In: *Annals Phys.* 97 (1976), p. 160. DOI: 10.1016/0003-4916(76)90225-6.

[34] Marc Henneaux, Axel Kleinschmidt, and Gustavo Lucena Gómez. “Remarks on Gauge Invariance and First-class Constraints.” In: *Ann. U. Craiova Phys.* 21 (2011), S1–S10.

[35] David J. Gross and Frank Wilczek. “Ultraviolet Behavior of Nonabelian Gauge Theories.” In: *Phys. Rev. Lett.* 30 (1973). Ed. by J. C. Taylor, pp. 1343–1346. DOI: 10.1103/PhysRevLett.30.1343.

[36] H. David Politzer. “Reliable Perturbative Results for Strong Interactions?” In: *Phys. Rev. Lett.* 30 (1973). Ed. by J. C. Taylor, pp. 1346–1349. DOI: 10.1103/PhysRevLett.30.1346.

[37] *Proceedings, Colloquium on Renormalization of Yang-Mills Fields, Marseille, June 19-23, 1972.* 1972.

[38] William E. Caswell. “Asymptotic Behavior of Nonabelian Gauge Theories to Two Loop Order.” In: *Phys. Rev. Lett.* 33 (1974), p. 244. DOI: 10.1103/PhysRevLett.33.244.

[39] D. R. T. Jones. “Two Loop Diagrams in Yang-Mills Theory.” In: *Nucl. Phys. B* 75 (1974), p. 531. DOI: 10.1016/0550-3213(74)90093-5.

[40] E. Egorian and O. V. Tarasov. “Two Loop Renormalization of the QCD in an Arbitrary Gauge.” In: *Teor. Mat. Fiz.* 41 (1979), pp. 26–32.

[41] Bernd A. Kniehl and Michael Spira. “Two loop O (alpha-s G(F) m(t)^2 correction to the $H \to b\bar{b}$ decay rate.” In: *Nucl. Phys. B* 432 (1994), pp. 39–48. DOI: 10.1016/0550-3213(94)90592-4. arXiv: hep-ph/9410319.

[42] Bernd A. Kniehl and Michael Spira. “Low-energy theorems in Higgs physics.” In: *Z. Phys. C* 69 (1995), pp. 77–88. DOI: 10.1007/s002880050007. arXiv: hep-ph/9505225.

[43] K. G. Chetyrkin, Bernd A. Kniehl, and M. Steinhauser. “Decoupling relations to O (alpha-s**3) and their connection to low-energy theorems.” In: *Nucl. Phys. B* 510 (1998), pp. 61–87. DOI: 10.1016/S0550-3213(97)00649-4. arXiv: hep-ph/9708255.

[44] Thomas Appelquist and J. Carazzone. “Infrared Singularities and Massive Fields.” In: *Phys. Rev. D* 11 (1975), p. 2856. DOI: 10.1103/PhysRevD.11.2856.

[45] K. G. Chetyrkin, Bernd A. Kniehl, and M. Steinhauser. “Strong coupling constant with flavor thresholds at four loops in the MS scheme.” In: *Phys. Rev. Lett.* 79 (1997), pp. 2184–2187. DOI: 10.1103/PhysRevLett.79.2184. arXiv: hep-ph/9706430.

[46] Y. Schroder and M. Steinhauser. “Four-loop decoupling relations for the strong coupling.” In: *JHEP* 01 (2006), p. 051. DOI: 10.1088/1126-6708/2006/01/051. arXiv: hep-ph/0512058.

[47] K. G. Chetyrkin, Johann H. Kuhn, and Christian Sturm. “QCD decoupling at four loops.” In: *Nucl. Phys. B* 744 (2006), pp. 121–135. DOI: 10.1016/j.nuclphysb.2006.03.020. arXiv: hep-ph/0512060.

[48] Robert V. Harlander and William B. Kilgore. “Next-to-next-to-leading order Higgs production at hadron colliders.” In: *Phys. Rev. Lett.* 88 (2002), p. 201801. DOI: 10.1103/PhysRevLett.88.201801. arXiv: hep-ph/0201206.

[49] Charalampos Anastasiou et al. "High precision determination of the gluon fusion Higgs boson cross-section at the LHC." In: *JHEP* 05 (2016), p. 058. DOI: 10.1007/JHEP05(2016)058. arXiv: 1602.00695 [hep-ph].

[50] S. Catani and M. H. Seymour. "A General algorithm for calculating jet cross-sections in NLO QCD." In: *Nucl. Phys. B* 485 (1997). [Erratum: Nucl.Phys.B 510, 503–504 (1998)], pp. 291–419. DOI: 10.1016/S0550-3213(96)00589-5. arXiv: hep-ph/9605323.

[51] Valentin Ahrens et al. "Origin of the Large Perturbative Corrections to Higgs Production at Hadron Colliders." In: *Phys. Rev. D* 79 (2009), p. 033013. DOI: 10.1103/PhysRevD.79.033013. arXiv: 0808.3008 [hep-ph].

[52] Charalampos Anastasiou et al. "Higgs Boson GluonFfusion Production Beyond Threshold in N^3LO QCD." In: *JHEP* 03 (2015), p. 091. DOI: 10.1007/JHEP03(2015)091. arXiv: 1411.3584 [hep-ph].

[53] Charalampos Anastasiou et al. "Higgs Boson Gluon-Fusion Production in QCD at Three Loops." In: *Phys. Rev. Lett.* 114 (2015), p. 212001. DOI: 10.1103/PhysRevLett.114.212001. arXiv: 1503.06056 [hep-ph].

[54] Charalampos Anastasiou et al. "Higgs boson gluon–fusion production at threshold in N^{3}LO QCD." In: *Phys. Lett. B* 737 (2014), pp. 325–328. DOI: 10.1016/j.physletb.2014.08.067. arXiv: 1403.4616 [hep-ph].

[55] Bernhard Mistlberger. "Higgs boson production at hadron colliders at N^{3}LO in QCD." In: *JHEP* 05 (2018), p. 028. DOI: 10.1007/JHEP05(2018)028. arXiv: 1802.00833 [hep-ph].

[56] Robert V. Harlander, Stefan Liebler, and Hendrik Mantler. "SusHi: A program for the calculation of Higgs production in gluon fusion and bottom-quark annihilation in the Standard Model and the MSSM." In: *Comput. Phys. Commun.* 184 (2013), pp. 1605–1617. DOI: 10.1016/j.cpc.2013.02.006. arXiv: 1212.3249 [hep-ph].

[57] Robert V. Harlander, Stefan Liebler, and Hendrik Mantler. "SusHi Bento: Beyond NNLO and the heavy-top limit." In: *Comput. Phys. Commun.* 212 (2017), pp. 239–257. DOI: 10.1016/j.cpc.2016.10.015. arXiv: 1605.03190 [hep-ph].

[58] D. de Florian et al. "Handbook of LHC Higgs Cross Sections: 4. Deciphering the Nature of the Higgs Sector." In: 2/2017 (Oct. 2016). DOI: 10.23731/CYRM-2017-002. arXiv: 1610.07922 [hep-ph].

[59] G. Das, S. Moch, and A. Vogt. "Approximate four-loop QCD corrections to the Higgs-boson production cross section." In: *Phys. Lett. B* 807 (2020), p. 135546. DOI: 10.1016/j.physletb.2020.135546. arXiv: 2004.00563 [hep-ph].

[60] Stefano Catani et al. "Soft gluon resummation for Higgs boson production at hadron colliders." In: *JHEP* 07 (2003), p. 028. DOI: 10.1088/1126-6708/2003/07/028. arXiv: hep-ph/0306211.

[61] George F. Sterman. "Summation of Large Corrections to Short Distance Hadronic Cross-Sections." In: *Nucl. Phys. B* 281 (1987), pp. 310–364. DOI: 10.1016/0550-3213(87)90258-6.

[62] S. Catani and L. Trentadue. "Resummation of the QCD Perturbative Series for Hard Processes." In: *Nucl. Phys. B* 327 (1989), pp. 323–352. DOI: 10.1016/0550-3213(89)90273-3.

[63] S. Catani and L. Trentadue. "Comment on QCD exponentiation at large x." In: *Nucl. Phys. B* 353 (1991), pp. 183–186. DOI: 10.1016/0550-3213(91)90506-S.

[64] Andreas von Manteuffel, Erik Panzer, and Robert M. Schabinger. "Cusp and collinear anomalous dimensions in four-loop QCD from form factors." In: *Phys. Rev. Lett.* 124.16 (2020), p. 162001. DOI: 10.1103/PhysRevLett.124.162001. arXiv: 2002.04617 [hep-ph].

[65] Christian W. Bauer, Dan Pirjol, and Iain W. Stewart. "Soft collinear factorization in effective field theory." In: *Phys. Rev. D* 65 (2002), p. 054022. DOI: 10.1103/PhysRevD.65.054022. arXiv: hep-ph/0109045.

[66] Christian W. Bauer et al. "Hard scattering factorization from effective field theory." In: *Phys. Rev. D* 66 (2002), p. 014017. DOI: 10.1103/PhysRevD.66.014017. arXiv: hep-ph/0202088.

[67] J. A. M. Vermaseren, A. Vogt, and S. Moch. "The Third-order QCD corrections to deep-inelastic scattering by photon exchange." In: *Nucl. Phys. B* 724 (2005), pp. 3–182. DOI: 10.1016/j.nuclphysb.2005.06.020. arXiv: hep-ph/0504242.

[68] S. Moch, J. A. M. Vermaseren, and A. Vogt. "The Longitudinal structure function at the third order." In: *Phys. Lett. B* 606 (2005), pp. 123–129. DOI: 10.1016/j.physletb.2004.11.063. arXiv: hep-ph/0411112.

[69] S. Moch, M. Rogal, and A. Vogt. "Differences between charged-current coefficient functions." In: *Nucl. Phys. B* 790 (2008), pp. 317–335. DOI: 10.1016/j.nuclphysb.2007.09.022. arXiv: 0708.3731 [hep-ph].

[70] S. Moch, J. A. M. Vermaseren, and A. Vogt. "Third-order QCD corrections to the charged-current structure function F(3)." In: *Nucl. Phys. B* 813 (2009), pp. 220–258. DOI: 10.1016/j.nuclphysb.2009.01.001. arXiv: 0812.4168 [hep-ph].

[71] J. Davies et al. "Non-singlet coefficient functions for charged-current deep-inelastic scattering to the third order in QCD." In: *PoS* DIS2016 (2016), p. 059. DOI: 10.22323/1.265.0059. arXiv: 1606.08907 [hep-ph].

[72] J. Blümlein et al. "The massless three-loop Wilson coefficients for the deep-inelastic structure functions F_2, F_L, xF_3 and g_1." In: *JHEP* 11 (2022), p. 156. DOI: 10.1007/JHEP11(2022)156. arXiv: 2208.14325 [hep-ph].

[73] H. Kawamura et al. "On the next-to-next-to-leading order QCD corrections to heavy-quark production in deep-inelastic scattering." In: *Nucl. Phys. B* 864 (2012), pp. 399–468. DOI: 10.1016/j.nuclphysb.2012.07.001. arXiv: 1205.5727 [hep-ph].

[74] Niccolò Laurenti. "Construction of a next-to-next-to-next-to-leading order approximation for heavy flavour production in deep inelastic scattering with quark masses." In: (Jan. 2024). arXiv: 2401.12139 [hep-ph].

[75] Julien Baglio et al. "Inclusive production cross sections at N^3LO." In: *JHEP* 12 (2022), p. 066. DOI: 10.1007/JHEP12(2022)066. arXiv: 2209.06138 [hep-ph].

[76] Claude Duhr, Falko Dulat, and Bernhard Mistlberger. "Charged current Drell-Yan production at N^3LO." In: *JHEP* 11 (2020), p. 143. DOI: 10.1007/JHEP11(2020)143. arXiv: 2007.13313 [hep-ph].

[77] Claude Duhr and Bernhard Mistlberger. "Lepton-pair production at hadron colliders at N^3LO in QCD." In: *JHEP* 03 (2022), p. 116. DOI: 10.1007/JHEP03(2022)116. arXiv: 2111.10379 [hep-ph].

[78] Xuan Chen et al. "Dilepton Rapidity Distribution in Drell-Yan Production to Third Order in QCD." In: *Phys. Rev. Lett.* 128.5 (2022), p. 052001. DOI: 10.1103/PhysRevLett.128.052001. arXiv: 2107.09085 [hep-ph].

[79] Xuan Chen et al. "Transverse mass distribution and charge asymmetry in W boson production to third order in QCD." In: *Phys. Lett. B* 840 (2023), p. 137876. DOI: 10.1016/j.physletb.2023.137876. arXiv: 2205.11426 [hep-ph].

[80] S. Moch et al. "Four-Loop Non-Singlet Splitting Functions in the Planar Limit and Beyond." In: *JHEP* 10 (2017), p. 041. DOI: 10.1007/JHEP10(2017)041. arXiv: 1707.08315 [hep-ph].

[81] S. Moch et al. "Low moments of the four-loop splitting functions in QCD." In: *Phys. Lett. B* 825 (2022), p. 136853. DOI: 10.1016/j.physletb.2021.136853. arXiv: 2111.15561 [hep-ph].

[82] J. Davies et al. "Large-nf contributions to the four-loop splitting functions in QCD." In: *Nucl. Phys. B* 915 (2017), pp. 335–362. DOI: 10.1016/j.nuclphysb.2016.12.012. arXiv: 1610.07477 [hep-ph].

[83] G. Falcioni et al. "The double fermionic contribution to the four-loop quark-to-gluon splitting function." In: *Phys. Lett. B* 848 (2024), p. 138351. DOI: 10.1016/j.physletb.2023.138351. arXiv: 2310.01245 [hep-ph].

[84] Thomas Gehrmann et al. "Complete N_f^2 contributions to four-loop pure-singlet splitting functions." In: *JHEP* 01 (2024), p. 029. DOI: 10.1007/JHEP01(2024)029. arXiv: 2308.07958 [hep-ph].

[85] G. Falcioni et al. "Four-loop splitting functions in QCD – The quark-quark case." In: *Phys. Lett. B* 842 (2023), p. 137944. DOI: 10.1016/j.physletb.2023.137944. arXiv: 2302.07593 [hep-ph].

[86] Thomas Gehrmann et al. "The NfCF3 contribution to the non-singlet splitting function at four-loop order." In: *Phys. Lett. B* 849 (2024), p. 138427. DOI: 10.1016/j.physletb.2023.138427. arXiv: 2310.12240 [hep-ph].

[87] T. Jaroszewicz. "Gluonic Regge Singularities and Anomalous Dimensions in QCD." In: *Phys. Lett. B* 116 (1982), pp. 291–294. DOI: 10.1016/0370-2693(82)90345-8.

[88] Richard D. Ball and Stefano Forte. "Summation of leading logarithms at small x." In: *Phys. Lett. B* 351 (1995), pp. 313–324. DOI: 10.1016/0370-2693(95)00395-2. arXiv: hep-ph/9501231.

[89] Richard D. Ball and Stefano Forte. "The Small x behavior of Altarelli-Parisi splitting functions." In: *Phys. Lett. B* 465 (1999), pp. 271–281. DOI: 10.1016/S0370-2693(99)01013-8. arXiv: hep-ph/9906222.

[90] Marco Bonvini and Simone Marzani. "Four-loop splitting functions at small x." In: *JHEP* 06 (2018), p. 145. DOI: 10.1007/JHEP06(2018)145. arXiv: 1805.06460 [hep-ph].

[91] Xin Guan et al. "Splitting amplitudes at N^{3}LO in QCD." In: *JHEP* 01 (2025), p. 090. DOI: 10.1007/JHEP01(2025)090. arXiv: 2408.03019 [hep-ph].

[92] J. McGowan et al. "Approximate N^{3}LO parton distribution functions with theoretical uncertainties: MSHT20aN^{3}LO PDFs." In: *Eur. Phys. J. C* 83.3 (2023). [Erratum: Eur.Phys.J.C 83, 302 (2023)], p. 185. DOI: 10.1140/epjc/s10052-023-11236-0. arXiv: 2207.04739 [hep-ph].

[93] Richard D. Ball et al. "The path to N^{3}LO parton distributions." In: *Eur. Phys. J. C* 84.7 (2024), p. 659. DOI: 10.1140/epjc/s10052-024-12891-7. arXiv: 2402.18635 [hep-ph].

[94] Thomas Cridge et al. "Combination of aN^{3}LO PDFs and implications for Higgs production cross-sections at the LHC." In: (Nov. 2024). arXiv: 2411.05373 [hep-ph].